Reviewed Preprint
v1 • March 31, 2025
Not revised

Reviewed Preprint
v2 • June 3, 2026
Revised by authors

Mapping Visual Contrast Sensitivity and Vision Loss Across the Visual Field with Model-Based fMRI

Hugo T Chow-Wing-Bom[a,b] ✉, Matteo Lisi[c], Noah C Benson[d], Freya Lygo-Frett[e], Patrick Yu-Wai-Man[a,f,g,h], Frederic Dick[b,i], Roni O Maimon-Mor[a], Tessa M Dekker[a,b,i]

[a]Institute of Ophthalmology, University College London (UCL), London, United Kingdom • [b]Birkbeck/UCL Centre for NeuroImaging, London, United Kingdom • [c]Department of Psychology, Royal Holloway, University of London, London, United Kingdom • [d]eScience Institute, University of Washington, Seattle, United States • [e]Institute of Cognitive Neuroscience, UCL, London, United Kingdom • [f]John van Geest Centre for Brain Repair and MRC Mitochondrial Biology Unit, Department of Clinical Neurosciences, University of Cambridge, Cambridge, United Kingdom • [g]Cambridge Eye Unit, Addenbrooke's Hospital, Cambridge University Hospitals NHS Foundation Trust, Cambridge, United Kingdom • [h]Moorfields Eye Hospital NHS Foundation Trust, London, United Kingdom • [i]Department of Experimental Psychology, UCL, London, United Kingdom

For correspondence: hugo.chow-wing-bom.15@ucl.ac.uk

Author notes: See page 33

Funding: See page 33

Reviewing editor: Xilin Zhang, Key Laboratory of Brain, Cognition and Education Sciences, Ministry of Education, South China Normal University, China

eLife Assessment

Using fMRI-based pRF mapping, this **important** study presents a novel method for estimating visual field (VF) loss and potential restoration by analyzing contrast-sensitivity patterns in early visual cortex. The evidence supporting the main claims is **convincing**. This work will be of broad interest to researchers in vision and clinical vision, neuroscience, and brain imaging.

https://doi.org/10.7554/eLife.105930.2.sa4

Abstract

Peripheral vision is crucial for daily activities and quality of life, yet traditional measures of visual function like visual acuity primarily assess central vision. Visual field tests can evaluate peripheral vision but require extended focus combined with precise fixation, often very challenging for patients with severe sight loss. Functional MRI (fMRI) with population receptive field (pRF) mapping offers a non-invasive way to map scotomas but is limited by its reliance on single contrast levels and the necessity of accurate fixation.

We developed an fMRI-based approach to measure contrast sensitivity across the visual field without the need for precise fixation. By combining large-field stimulation with varying spatial frequencies and contrast levels with either pRF mapping or a retinotopic atlas based on anatomical landmarks, we modeled contrast sensitivity in the primary visual cortex (V1) over a large (40 deg) expanse of the visual field. In seven normal-sighted participants, we characterized differences in V1 cortical sensitivity across eccentricities and visual quadrants, finding reliable and reproducible patterns of sensitivity differences at individual and session levels. To assess the method's tolerance to fixation variability, we further investigated how different levels of eye movement affect cortical sensitivity patterns in two participants. We found that cortical sensitivity patterns were largely preserved across eye movement, particularly at low spatial frequencies. This suggests that our approach can accommodate several degrees of fixation instability, making it suitable for populations with unstable or biased fixation for whom visual field maps are harder to acquire behaviorally (e.g., patients with dense central scotoma or strabismus). Additionally, our method effectively visualized cases of simulated and disease-linked sensitivity loss at the cortical

level. Crucially, we demonstrated that these results could be largely recovered using a structure-based retinotopic atlas, eliminating the need for pRF mapping and precise fixation - although such an approach reduced sensitivity.

This approach, integrating large-field stimulation with a retinotopic atlas, offers a promising tool for monitoring vision loss and recovery in patients with various visual impairments, addressing a significant challenge in current clinical assessments.

Introduction

At least 2.2 billion people world-wide experience blinding eye diseases that emerge or progress across the lifespan, with 1.1 billion living with vision loss in 2020 (Bourne et al., 2021; World Health Organization, 2019). Accurate characterization of visual function is critical for optimal intervention and patient support, but fraught with challenges. The gold clinical standard measure is visual acuity, the highest spatial resolution that can be discerned. This index mainly relies on a well-functioning fovea, the small retinal area with the highest density of photoreceptors, which processes the central 0-2 degrees around fixation. However, many forms of visual impairment do not affect the fovea alone. The vast majority of our visual input comes from peripheral vision, which provides coarse but invaluable information (Alvarez, 2011; Oliva, 2005) – nearly all daily functions critically depend on intact functionality of the wider visual field, including driving, crossing the street, social function, mobility, and even reading (Lange et al., 2021). Accordingly, impairment of tissue beyond the fovea and its projections drastically affects function and quality of life (Lange et al., 2021; Lisboa et al., 2013; Roh et al., 2018; Subhi et al., 2017). Still, testing visual function across the visual field remain limited in clinical and therapeutic contexts, especially in patients with drastic central vision loss. In this study, we aimed to address this gap by introducing a novel fMRI-based approach to measure visual field sensitivity across a wide expanse of the visual field (40° diameter).

Beyond visual acuity, functional impairment across the wider visual field can be measured using a range of visual field tests, from the finger counting visual confrontation field test to more complicated and/or computerized tests (e.g., standard automatic perimetry, kinetic perimetry, microperimetry; Rai et al., 2024). Computerized tests typically involve measuring sensitivity to the luminance contrast of a target relative to a background at different visual field locations while the participant's gaze is fixed on a central point. In some cases (e.g., microperimetry), sensitivity measurements are paired with fundus imaging, offering greater precision in linking visual field functions to specific retinal locations (Rai et al., 2024). As a result, visual field assessments can reveal functionally relevant deficits – including localized sensitivity loss and scotomas – that are not captured by foveal acuity alone, and are therefore potentially valuable for tracking disease progression and therapeutic efficacy.

Despite their clinical relevance, visual field testing comes with challenges and limitations, and as a result, the inclusion of visual field measures in sight-rescuing therapy trials is limited. Firstly, it requires prolonged fixation and sustained visual attention. This can be very challenging for patients with severe vision loss, who often struggle to fixate, and strain to detect even high-intensity stimuli. This can lead to long and unpleasant testing sessions with unreliable results. Secondly, as perception of light stimuli is inherently subjective (Rai et al., 2024) and effortful, patients may vary in their criteria for visual recognition, and in their ability to report visual signals that are weakened or distorted by disease. Together, these constraints reduce the feasibility, robustness, and interpretability of conventional visual field testing in clinical trials, underscoring the need for alternative or complementary approaches that can assess functional vision while placing fewer demands on subjective reporting.

Functional MRI (fMRI) has recently been proposed as a promising alternative to measure visual field loss, as it requires no overt task, and instead measures visual sensitivity directly from brain responses (Farahbakhsh et al., 2022; Prabhakaran et al., 2021; Ritter et al., 2019). Population receptive field (pRF) mapping fMRI can measure which parts of the cortex respond to which parts of the visual scene (Dumoulin & Wandell, 2008). This is achieved by measuring local changes in

cortical blood oxygenation in response to high-contrast stimuli such as flickering checkerboards that systematically traverse the visual field. These neural timeseries are then fit with a retinotopic spatial tuning function. The fMRI signal strength in a cortical region that encodes a specific visual field location provides information about visual sensitivity in this location (Dumoulin & Wandell, 2008). This approach has recently been used to accurately recover blind spots in the visual field detected with visual field perimetry (Pawloff et al., 2023; Ritter et al., 2019). These results in turn suggest that fMRI may be a useful tool to monitor disease progression and recovery in visually impaired patients.

However, there are also significant challenges associated with this pRF mapping. Because pRF models require knowledge of where visual stimuli fall on the retina, this approach requires accurate and sustained fixation. If fixation is poor, the visual field locations assigned to cortical regions will be displaced, leading to noise or bias in the pRF maps. Additionally, most fMRI studies measure vision across a small central part of the visual fields (~10 degrees of eccentricity) which will not capture critical dynamics in the periphery. Finally, most studies use a single maximum contrast stimulus to assess visual function (Broderick et al., 2022; Farahbakhsh et al., 2022; Liu et al., 2006; O'Connell et al., 2016; Ritter et al., 2019). This is suboptimal for at least two reasons: First, it may reduce the ability to detect subtle but clinically important changes that do not result in complete sensitivity loss or recovery. Second, with a single contrast stimulus, it becomes more difficult to determine whether a reduction in fMRI signal across sessions or brain regions reflects vision-related changes or other factors. Together, these factors currently limit the utility of neuroimaging-based visual field tests.

In this study we sought to develop fMRI methods for measuring visual field sensitivity to address these challenges, and to test its utility in artificial and realistic cases of visual field loss. Rather than presenting a single maximum contrast eccentricity-scaled checkerboard in a pRF mapping protocol, observers viewed large-field sinusoidal gratings at a range of contrasts without strict requirement to fixate. We used a large screen set up (40° diameter) to measure visual function across a large expanse of the visual field. To quantify visual sensitivity, we fit a simple cortical contrast response model to voxel timeseries evoked by the gratings, avoiding reliance on arbitrary signal amplitude thresholds. We first tested if this approach could sensitively and reliably quantify predicted contrast sensitivity differences across eccentricity and polar angle dimensions of the entire visual field (Figure 1), using a short, patient-friendly protocol in sighted controls. Critically, to achieve this we linked cortical contrast sensitivity estimates to visual field locations using retinotopic tuning estimates obtained in a separate session. However, for patients with severe vision loss it is infeasible to obtain accurate pRF measures due to poor ability to fixate a central target. We therefore also evaluated the approach using the structure-based atlas of retinotopic values developed by Benson et al. (Benson et al., 2014; Benson & Winawer, 2018). This atlas predicts retinotopic organization by aligning individual cortical anatomy (e.g., surface curvature) to a group-average template that incorporates an algebraic model of retinotopy (Benson et al., 2014). Once the subject's brain is aligned to this structural atlas, retinotopic maps defined by the model – i.e., polar angle and eccentricity maps – are projected onto the individual's cortex. This allows estimation of visual field maps without requiring functional imaging, and provides a non-invasive, anatomy-driven approximation of visual field representations. To increase accuracy of the Benson atlas for our large-field stimuli, we subsequently fit these eccentricity estimates to the Horton and Hoyt (1991) model of cortical magnification in each individual.

We demonstrate that our approach can recover, at a cortical level, known sensitivity changes across the visual field. V1 neuronal populations encoding the central visual field show the highest sensitivity to high spatial frequencies, whilst those encoding the periphery are most sensitive to low spatial frequencies. We also find greater sensitivity in V1 regions receiving visual inputs from the horizontal compared to vertical quadrants, and from the lower compared to upper quadrants. Crucially, these effects are detectable at the individual level and repeatable across visits, suggesting our approach will be suitable for detecting visual field sensitivity changes over time (e.g., due to learning, ageing, disease progression, or recovery). Moreover, when using the Benson

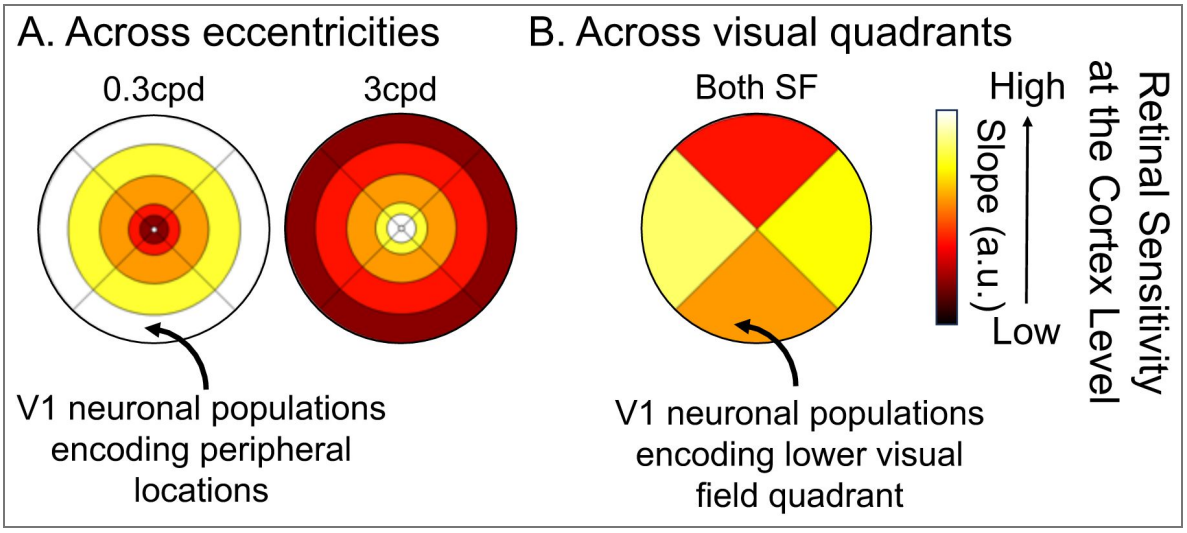

Figure 1. Expected changes in cortical contrast sensitivity in typically sighted controls for two different spatial frequencies (low spatial frequency, 0.3 cycles per degree (cpd), and high spatial frequency, 3.0 cpd), A: as a function of eccentricity and B: visual field quadrants.

With reference to eccentricity, we expect higher sensitivity of V1 neuronal populations to 1) lower spatial frequencies in the periphery, and 2) higher spatial frequencies in the center of the visual field. By comparison, we expect both high and low spatial frequency stimulation to evoke greatest sensitivity in V1 neuronal populations encoding the left and right visual quadrants, less in the lower, and least in the upper quadrant.

atlas instead of individual pRF measures to link neuronal responses to visual field locations, we still detect these effects, although with slightly reduced sensitivity. We also demonstrate the clinical relevance of this approach by recovering simulated scotomas (i.e., a ring of visual field loss around fixation and the loss of an entire visual field quadrant), as well as visual field loss in a patient with a neurodegenerative disorder causing large areas of visual field loss. We conclude that this approach, i.e., the combination of cortical contrast sensitivity testing, large field stimulation, and a large-field calibrated retinotopic atlas, may be particularly useful for quantifying visual recovery in patients, whether spontaneous or following gene-therapy interventions, and for linking brain-based activations to behavioral performance.

Methods

Participants

We collected data from 7 healthy controls (mean±SD: 29.6±4.7yo; 1M). All controls either had normal or corrected to normal vision, with no other ocular pathologies, and were recruited from the local staff and student pool at the University College of London. Each control completed both the population receptive field (pRF) mapping and the fMRI contrast sensitivity task. To assess measurement repeatability, four participants (C2, C4, C5, C6) performed the contrast sensitivity task twice. Additionally, one participant (C5) repeated the task under two simulated vision loss conditions (ring or quadrant loss), and two others (C5, C6) completed it with different levels of eye movement.

We also recruited a patient with Leber Hereditary Optic Neuropathy (M, 45.5 years old, mutation: m.11778G>A, disease duration: 36.1 years), who presented with relatively stable fixation and was able to complete both the pRF mapping and the fMRI contrast sensitivity task. All participants signed a written informed consent to participate in the study, and this study was approved by HRA/HCRW and Research Ethics Committee (IRAS 258959; REC 20/YH/0336).

Stimulus & Apparatus

Stimuli were programmed in MATLAB 2020b (MathWorks, Natick, Massachusetts, USA) using the Psychtoolbox-3, and displayed using an EPSON LB-1100U projector (resolution: 1920x1200 pixels, 60Hz, projected area: 43.2x27cm). Because the projector was too bright and to reduce discomfort in the scanner, a circular neutral density filter (ND4 Plus+; Urth, Byron Bay, Australia) was placed in front of the projector to reduce light intensity by 4 times without altering the colors. The projector was also gamma-corrected to ensure accurate representation of the intended contrast levels and spatial frequencies used in our experiments. In all tasks, stimuli were embedded in circular aperture of 42.3x42.3° diameter. To achieve the large field-of-view, the front part of the 64-channel MRI coil was removed, and stimuli were back-projected onto a screen positioned close to the participant's head inside the bore (see Figure A1 in *Appendix* section). Participants viewed the stimuli through a mirror, for a total viewing distance of 34cm. Throughout the session, participants were constantly reminded to remain still to minimize head and body motion, and eye motion and alertness were monitored using an EyeLink 1000Plus device (SR Research, Ottawa, Canada). In all tasks, participants were asked to report when the color of a central fixation dot changed.

fMRI Contrast Sensitivity Task

Participants were presented binocularly with achromatic sine-wave gratings, flickering at a temporal frequency of 2Hz and varying in contrast levels and spatial frequencies. Contrast levels were defined as Michelson contrast $\left(C = \frac{L_{\max} - L_{\min}}{L_{\max} + L_{\min}}\right)$, where Lmax and Lmin are maximum and minimum luminance. Each stimulus, presented for 13s, featured a specific contrast level (either 7.5, 42.2, 60, or 100%) and spatial frequency (either 0.3 or 3 cycles per degree). Stimuli were then followed by 2s of a grey background (0% contrast) to minimize the experience of after-effects. Each combination of contrast level and spatial frequency was shown three times within a run, arranged in a pseudo-random sequence, for a total of 9 repetitions per combination (i.e., 3 runs). Eight

additional blocks of 15-second rest periods with a grey background were introduced to allow sufficient baseline. Four participants (C2, C4, C5, C6) were invited for a second session in which they repeated the task to assess the reliability of the measures.

For six control participants (C1–C6), gratings were initially presented with a fixed horizontal orientation. In an updated version of the task – used for C7, cases of simulated eye movement, cases of artificial scotoma, and the LHON patient – the orientation varied every 5 s among four angles (−45°, 0°, 45°, 90°). Contrast sensitivity patterns were consistent across single- and multiple-orientation conditions, including in participants who completed both versions, indicating robustness across orientation-tuned populations.

Effect of eye movement

Participants C5 and C6 also performed a version of the task designed to test the effect of eye movements. In this version, saccades were elicited by randomly and rapidly shifting the fixation dot away from central fixation (C5: 2° and 5° from fixation and random motion; C6: up to 2° from fixation). Participant C5 was tested using 0.3 and 3cpd gratings at four contrast levels (7.5, 42.2, 60, 100%), while participant C6 was tested only under the low spatial frequency condition (0.3cpd).

Fixation stability was assessed for each fMRI run using the bivariate contour ellipse area (BCEA), which estimates the area (in degrees² or arcmin²) of an ellipse that contains approximately 95% of fixation points. BCEA was calculated using the formula: $BECA = 2 * k * \pi * \sigma_h * \sigma_v * \sqrt{1-\rho^2}$, as described by Morales et al. (2016). In this expression, σ_h and σ_v represent the standard deviations of eye position in the horizontal and vertical directions, respectively, while ρ corresponds to the Pearson correlation coefficient between horizontal and vertical eye positions. The constant k determines the size of the ellipse based on the desired probability area, defined by the relationship $P = 1 - e^{-k}$, with P set to 0.95 in this study. A smaller BCEA indicates greater fixation stability.

Simulated vision loss

One healthy control participant (C5) also performed a version of the task designed to simulate two forms of visual input loss (i.e., artificial scotoma). These simulations were implemented by: (a) masking a region of the visual field with a grey, annular ring, covering 3°-8° eccentricity, and (b) masking the upper-right visual quadrant using a grey quarter-sector overlay. The stimuli and contrast levels used in this task were identical to those described in the original task.

Population Receptive Field (pRF) mapping

To investigate how distinct regions of the visual field map onto the cortex, we collected pRF mapping data using a standard ring-and-wedge stimulus (Dumoulin & Wandell, 2008). Participants were presented binocularly with a black-and-white checkerboard, phase-flickering at a temporal frequency of 2Hz, and at maximum contrast level. The stimulus spanned up to the boundaries of the circular aperture (i.e., 42.3x42.3° diameter) and was scaled across eccentricity to account for cortical magnification. This scaling was implemented by applying a logarithmic transformation of retinal radius, such that radial checker boundaries were defined in log-eccentricity space ($log(r)$, where r denotes to eccentricity relative to the fixation target). This produced an exponential increase in checker size with eccentricity (scaling factor = 3.2; ~1.37 times increase per radial step), resulting in lower spatial-frequency content at larger eccentricities – consistent with known variations in V1 spatial-frequency tuning. Because this eccentricity-dependent scaling assumes precise fixation, it can be challenging for individuals with central vision loss, further motivating the use of Benson atlas templates in such populations. Three runs of 352 volumes were collected per participant.

MRI acquisition

Data were collected at the Birkbeck-UCL Centre for NeuroImaging (BUCNI, London, UK), on a Siemens PRISMA 3 Tesla scanner.

Functional data were acquired using a 64-channel head coil with the front part removed, to allow an unobstructed view of the screen whilst ensuing enough signal from the remaining 40 effective channels covering the side and back of the head. T2*-weighted echo-planar imaging were collected with an accelerated multiband sequence kindly provided by CMRR (version R016a, *https://www.cmrr.umn.edu/multiband*; Cauley et al., 2014; Xu et al., 2013); multi-band factor: 4, voxel resolution: 2mm isotropic, FOV: 212x212x96mm, flip angle: 60°, repetition time (TR): 1000ms, echo time (TE): 35.2ms, echo spacing: 0.56ms, bandwidth: 2620Hz/Px, with 48 transverse slices angled to be approximately parallel to the calcarine sulcus whilst avoiding the orbital cavities). The same sequence was used to acquire 4 additional scans in the opposite phase-encoding direction, to allow B0 deformation correction in the pre-processing steps.

A T1-weigthed structural image was acquired with a 32-channel coil, using MPRAGE sequence (voxel resolution: 1mm isotropic, 208 slices, FOV: 256 x 256 x 208mm, flip angle: 7°, TR = 2300ms, TE = 2.98ms, TI = 900ms, bandwidth: 240Hz/Px, echo spacing: 7.1ms, acquisition time: 5min30s).

Data analysis

Segmentation of the anatomical scan and reconstruction of cortical surfaces were performed in FreeSurfer 7.1.1.

Functional data were pre-processed using a combination of AFNI 24.1.22, FreeSurfer and FSL 6.0.7.12 commands. The following steps were followed for both the contrast sensitivity task and the pRF mapping task. First, initial correction for distortions caused by field inhomogeneity was performed using a blip-up/blip-down approach (AFNI's unWarpEPI.py program), and the first 4 volumes of each run were discarded using FSL's fslroi program. Then an alignment scan was created from the volume out of all collected runs that contained the least amount of voxel outliers using AFNI's 3dToutcount, 3dTstat and 3dcalc programs. This alignment scan was then co-registered to the MPRAGE image using FreeSurfer's bbregister program, resulting in a rigid-body transformation matrix. In case of misregistration, the alignment scan was defined as one of the single-band reference scans, before re-running the co-registration step. Motion correction was then carried out by aligning each functional volume from all runs to the previously defined alignment scan using AFNI's 3dvolreg program.

Processing of the contrast sensitivity task

To accurately capture neural activity across various eccentricities and polar angle locations, minimal smoothing (0.5mm FWHM Gaussian blur) was applied to the contrast sensitivity task data using FSL's 3dmerge program. This was done to meet the minimum requirements of the GLM module in SPM. The contribution of each contrast/spatial frequency combination to the BOLD signal was modelled using the general linear model (GLM) approach in SPM12 (*https://www.fil.ion.ucl.ac.uk/spm/*), with motion parameters as additional regressors. This step resulted in volumetric images of β-values, each reflecting the specific contribution of a given contrast/spatial frequency combination to the baseline BOLD signal. These resulting β-images were then projected onto the individual's cortical surface using FreeSurfer's mri_vol2surf program, with no surface smoothing and the default fractional projection along surface of 0.5. The latter sets the fraction (0,1) of the cortical thickness at each vertex to project along the surface. Surface-projected β-images were finally converted into a MATLAB-compatible format for further analysis using SamSrf's samsrf_mgh2srf program.

Processing of pRF mapping task

Pre-processed volumes from the pRF mapping task were projected onto the cortical surface using FreeSurfer's mri_vol2surf program. Here, we used the previously generated rigid-body transformation matrix to ensure accurate spatial alignment and smoothed on the cortical surface with a Gaussian kernel with a FWHM of 3mm.

During pRF model fitting, pRF centers were allowed to extend beyond the stimulated visual field to improve model stability near stimulus boundaries – up to approximately 1.5 times the maximum stimulus eccentricity (~30°). Eccentricity was sampled on a logarithmically spaced grid defined as

$2^{)}$, with x ranging from −5 to 0.6 in steps of 0.2, and then scaled by the maximum stimulus eccentricity (20°) to express pRF centers in degrees of visual angle. This sampling scheme provided finer resolution near the fovea and progressively coarser sampling at larger eccentricities, consistent with cortical magnification principles.

The resulting outputs were then converted into a MATLAB-compatible format for further analysis. pRF estimates were computed by fitting a 2D Gaussian model to the data, using the SamSrf toolbox (version 7.13; *https://github.com/samsrf*), resulting in three pRF parameters for each vertex on the cortical surface: the x- and y-coordinates of the pRF center, and the pRF size (σ). Eccentricity and polar angle maps were computed from the x- and y-coordinates.

Regions-Of-Interest

In this study, we were interested in how visual information across the visual field is processed in early visual areas, notably in the primary visual cortex V1. Early visual regions were manually delineated for each participant in SamSrf v7.13, based on the output of the pRF fitting procedure and standard functional criteria to identify borders between V1, V2, and V3 (DeYoe et al., 1996; Engel, 1997; Sereno et al., 1995). In this report, we focused our interest on V1, given its crucial role in the initial processing of basic visual features like spatial frequency and contrast. For all subsequent analyses of cortical contrast sensitivity, pRF centers outside the stimulated 20° eccentricity were excluded. Similarly, although the Benson atlas provides eccentricity estimates extending far beyond the stimulated range (up to ~90°), only values within 20° were retained to maintain consistency across pRF-based and atlas-based analyses.

Quantifying eccentricity- and location-dependent variations in sensitivity

Using subject-specific pRF estimates

At this stage, for each vertex on the cortical surface, we obtained β-values for each tested contrast/spatial frequency combination in the contrast sensitivity task, as well as pRF parameters resulting from the fitting of the pRF model to the pRF data (Figure 2). β-values from the contrast sensitivity task in each vertex were then filtered based on ROI location (V1) and pRF parameters ($R^2 \geq 0.05$; pRF size: $\sigma \leq 6$).

To assess contrast sensitivity, we modelled the neural response (i.e., β-values) in V1 as a linear function of the square root of the contrast values ($R(C) = a * \sqrt{C}$). This model rests on the assumption of a monotonic relationship between the presented stimulus contrast level and the resulting BOLD response and has been used in previous work by Buracas and colleagues to investigate contrast sensitivity at the cortex level in healthy controls (Buracas et al., 2005; Buracas & Boynton, 2007). Steeper slopes within this context indicate greater V1 contrast sensitivity.

We fit this model for each vertex separately, for each participant and spatial frequency (0.3 and 3cpd) condition. The intercept was constrained to be zero, as the distribution of β-values is expected to be centered on zero when the contrast is zero (i.e., when no stimulus is presented). Next, the resulting V1 slope estimates were binned and averaged over five regions using pRF eccentricity estimates: 0.5°-2.5°, 2.5°-4.5°, 4.5°-9.5°, 9.5°-15°, and 15°-20°. These bins relate to the clinical definition of visual space based on anatomical landmarks, corresponding to the fovea, parafovea, perifovea and two near-periphery regions, respectively. Similarly, slope estimates were spatially constrained within a ±45°-wedge centered on each cardinal meridian to investigate asymmetries as a function of pRF polar angle locations, thus dividing the visual space between the upper, lower, left and right quadrants. These wedges were also derived from the polar angle estimates obtained with pRF mapping.

For each participant, average slopes for each eccentricity bin and polar angle wedge were then projected back into their corresponding visual field locations. This resulted in heat-maps of V1 contrast sensitivity across eccentricities and visual field quadrants, for each tested spatial

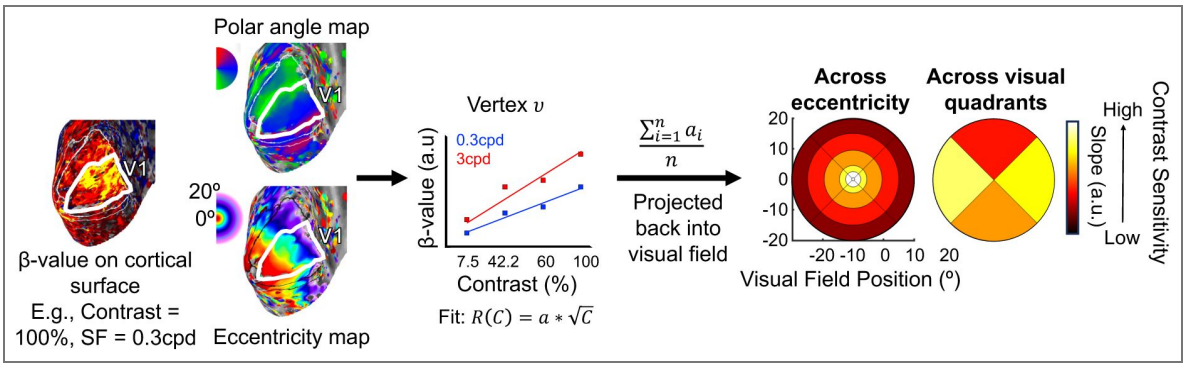

Figure 2. Estimation of cortical contrast sensitivity across the visual field.

Participants performed two fMRI tasks in the scanner: a contrast sensitivity task and a pRF mapping task. For each individual and tested spatial frequency, the contribution of each stimulus contrast level to the BOLD signal in the contrast sensitivity task was estimated using a GLM approach. Resulting β-coefficients for each contrast level were then projected onto the individual's cortical surface. For each vertex in V1, a square root function ($R(C) = a * \sqrt{C}$) was then fitted to these data, taking the estimated slope a as measure of cortical contrast sensitivity. V1 slopes were finally averaged across vertices based on their eccentricity and polar angle preference as estimated with pRF mapping, and across participants. Mean slopes were then projected back into the visual space, producing a heatmap projection of V1 contrast sensitivity across eccentricities and along visual field quadrants.

frequency condition at an individual level (Figure 2). Finally, average slopes for each eccentricity and polar angle bin from each participant were used to compute the group-level average.

Using calibrated Benson retinotopic template atlas

The same approach was used to quantify changes in V1 contrast sensitivity across the visual field, using a retinotopic template (Benson et al., 2014; Benson & Winawer, 2018) instead of pRF mapping. This template was fitted to each subject's anatomical MPRAGE image using the Python library neuropythy (Benson & Winawer, 2018), which provided automatic delineation of early visual regions, based on FreeSurfer's anatomical alignment. Additionally, it offered eccentricity and polar angle estimates for each vertex on the cortical surface. The advantage of this method over pRF mapping is that it does not require fixation or pRF scanning, making it a valuable tool to use when scan time is valuable or in populations where good fixation is hard to achieve.

We initially observed inaccuracies between the template and individual retinotopy eccentricity estimates which led to substantial distortions in cortical visual field maps due to cortical magnification – especially in peripheral locations (see Figure A4 in *Appendix* section). To enhance the accuracy of eccentricity estimates in the template map, we aligned the distribution of eccentricity values from the fitted Benson template atlas with Horton and Hoyt's model (Horton & Hoyt, 1991; Figure 3A). This model suggests that the linear cortical magnification factor (M_{linear} in mm/°) is inversely proportional to eccentricity (E in degrees), expressed as $M_{\text{linear}} = \frac{\text{scale}}{E+\text{ shape}}$, with the normalizing parameter s□□□□ equal to 0.75°, as measured by Horton and Hoyt (1991). Using this relationship, we first estimated for each hemisphere the *scale* value based on each individual's V1 surface area (from the Benson V1 label) and the minimum and maximum eccentricities considered in the model (0° and 90°). The mean *scale* value for the left and right V1 hemispheres across all tested controls were 15.0±0.99 and 16.0±1.09, respectively. In comparison, Horton and Hoyt (1991) measured a mean *scale* of 17.3 mm. The mean V1 surface areas for the left and right hemispheres were 2700.7±358.7mm^2 and 3067.7±416.3mm^2.

We then defined a function $f(r)$ that describes how the surface area of V1 changes with eccentricity (Equation 1; Figure 3A). This was achieved by integrating Horton and Hoyt's function over the visual field, resulting in an equation that calculates the amount of V1 surface area from the foveal confluence up to a particular eccentricity (r). Next, we sorted the input eccentricity values and calculated the cumulative surface areas. A numerical method was then employed to find the eccentricity values that match the desired distribution. This method involved iteratively adjusting the range of possible values until the calculated values closely matched the desired values. Finally, the adjusted eccentricity values were returned in their original order and values from both hemispheres were merged to provide bilateral eccentricity estimates.

$$f(r) = \pi * \text{scale}^2 * \left(\log\left(\frac{r+\text{ shape}}{\text{shape}}\right) - \frac{r}{r+\text{ shape}}\right) \quad (1)$$

Results

To measure visual field function, we developed a new measure of cortical contrast sensitivity, assessing the brain's ability to discriminate gratings of varying spatial frequencies based on luminance variations. This depends on many factors, including the size, orientation, and density of cells in different parts of the retina. As these factors change across the visual field, contrast sensitivity varies with spatial frequency and visual field location in the typical, healthy visual system. We first investigated whether our brain-based approach can reliably detect these known differences in contrast sensitivity as a function of eccentricities and visual field quadrants, in individual normal sighted controls. We then investigated whether our approach could recover loss of visual inputs at the cortical level, either simulated in a healthy control or pathological in a patient. In each section, findings were first reported for the pRF-defined ROIs and then for the Benson-defined ROIs.

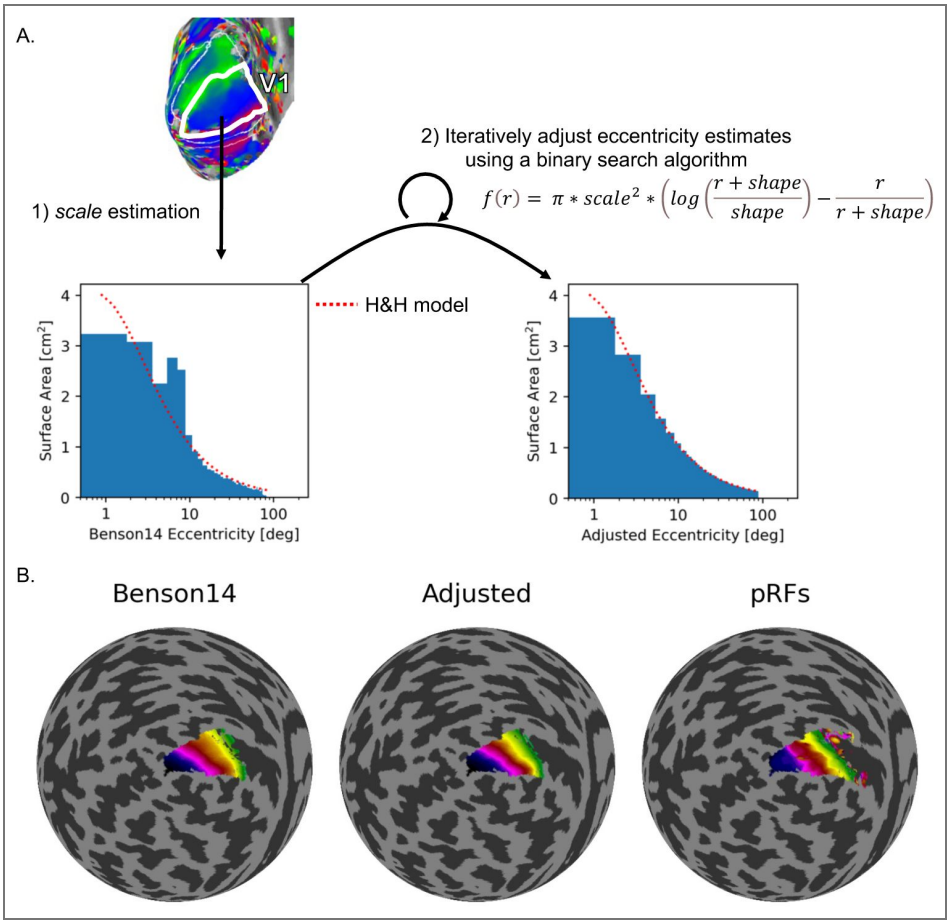

Figure 3. Eccentricity alignment and surface area estimation in V1.

A: For each hemisphere, the scale parameter in Horton and Hoyt's linear magnification model $M_{\text{linear}} = \frac{\text{scale}}{E+0.75}$ was estimated from individual V1 surface area and the 0°-90° eccentricity range. Using this, we derived a cumulative surface-area function $f(r)$, which gives the total cortical area of V1 representing eccentricities from 0° to r. For visualization, the histograms show the differential form of this function – i.e., the surface-area density as a function of eccentricity. This corresponds to the derivative $\frac{df}{dr}$, which reflects the areal magnification (denoted $m*(r)$) integrated over polar angle. This representation provides a clearer view of how cortical surface area is distributed across eccentricities while remaining consistent with the underlying cumulative function $f(r)$. Adjusted eccentricity values were obtained by iteratively matching the empirical surface-area distribution to the model using a binary search procedure. **B:** Comparison of eccentricity maps generated using the Benson template, the adjusted eccentricity values, and population receptive field (pRF) estimates, showing improved alignment with empirical data.

Spatial frequency preference changes in V1 neuronal populations across eccentricities

For high spatial frequency stimuli, we expected better sensitivity in V1 neuronal populations encoding central locations in visual space than in those encoding the periphery. In contrast, for low spatial frequency information, we expected the opposite, better sensitivity in V1 neuronal populations encoding the periphery than the center of the visual field.

Using ANOVA, we found the expected interaction between spatial frequency and eccentricity ($F(1.96,11.79) = 28.66$, $p < 0.001$; Figure 4) as well as a main effect of eccentricity ($F(2.33,13.99) = 12.67$, $p < 0.001$). These effects were statistically significant at the individual participant level showing high sensitivity (Figure 4A, transparent lines show individual data; Figure 4C shows individual visual field plots; for stats, see Table A1 in *Appendix* section).

Post-hoc tests using Holm-Bonferroni correction show that V1 neuronal populations receiving inputs from the central visual field (0.5-4.5°) showed greater contrast sensitivity to high spatial frequency as compared to low spatial frequency stimuli (steeper slope for the 3cpd versus 0.3cpd condition: **0.5-2.5°**: $t(6) = 4.35$, $p_{45,6} = 0.0149$; **2.5-4.5°**: $t(6) = 3.471$, $p_{45,6} = 0.0266$). Conversely, peripheral eccentricities in V1 (above 9.5°) showed higher contrast sensitivity to low as compared to high spatial frequency stimuli (steeper slope for 0.3cpd versus 3cpd condition: **9.5-15°**: $t(6) = -4.591$, $p_{45,6} = 0.0149$; **15-20°**: $t(6) = -6.615$, $p_{45,6} = 0.0029$). Between 4.5° and 9.5°, V1 contrast sensitivity was similar for both spatial frequencies ($t(6) = -0.226$, $p_{45,6} = 0.8286$). Crucially, these effects remained when using retinotopic estimates based on structural scans derived from the Benson retinotopic atlas instead of the pRF-mapping measures (**0.5-2.5°**: $t(6) = 5.768$, $p_{45,6} = 0.0059$; **2.5-4.5°**: $t(6) = 2.531$, $p_{45,6} = 0.0892$; **4.5-9.5°**: $t(6) = -0.293$, $p_{45,6} = 0.7792$; **9.5-15°**: $t(6) = -3.274$, $p_{45,6} = 0.0509$; **15-20°**: $t(6) = -3.528$, $p_{45,6} = 0.0496$; see Figure A2 and Table A3 in *Appendix* section).

These results demonstrate that our approach can detect subtle changes in visual sensitivity across eccentricities at the individual participant level. The ability to reveal these gradients was made possible by the large peripheral coverage provided by our large-field stimulation set-up (see Figure A1 in *Appendix* section), which enabled a more complete characterization of V1 sensitivity across the visual field. Importantly, the same effects were preserved when using retinotopic estimates derived from structure-based atlases, demonstrating that atlas-based methods can be used as alternative to pRF mapping in cases where it might otherwise be difficult or impossible to directly collect pRF measures. Together, these highlight both the validity of our approach and its potential to broaden the scope of visual neuroscience.

Contrast sensitivity is not equal across the visual field quadrants in V1 neurons

Contrast sensitivity is known to vary across the quadrants of the visual field; Previous behavioral studies have shown greater contrast sensitivity along the horizontal versus vertical meridians, and along the lower versus upper vertical meridian (Barbot et al., 2021; Carrasco et al., 2022; Himmelberg et al., 2020, 2023). Recent fMRI studies have also shown that these asymmetries in BOLD response amplitude to single contrast gratings (Kurzawski et al., 2022; Liu et al., 2006; O'Connell et al., 2016). Therefore, we expect our fMRI approach to uncover these established asymmetry patterns at the cortical level.

Figure 5 shows how cortical contrast sensitivity in V1 varies across visual field quadrants, for the 0.3cpd and 3cpd conditions. For this analysis, we collapsed eccentricities (0.5° to 20°) into a single bin. We found a main effect of visual field quadrant location on V1 sensitivity ($F(2.46,14.76) = 20.71$, $p < 0.001$). Post-hoc pairwise comparisons using Holm-Bonferroni corrections revealed that, as predicted, the cortical contrast response function had a higher slope – indicating better V1 sensitivity – along the horizontal versus vertical quadrants (Horizontal-Vertical Anisotropy – **HVA:** $t(6) = 5.908$, $p_{45,6} = 0.0031$) and along the lower versus upper quadrant (Vertical Meridian Anisotropy – **VMA:** $t(6) = 4.106$, $p_{45,6} = 0.0126$). Conversely, no difference in cortical contrast sensitivity was found between V1 neuronal populations encoding the left and right quadrants of

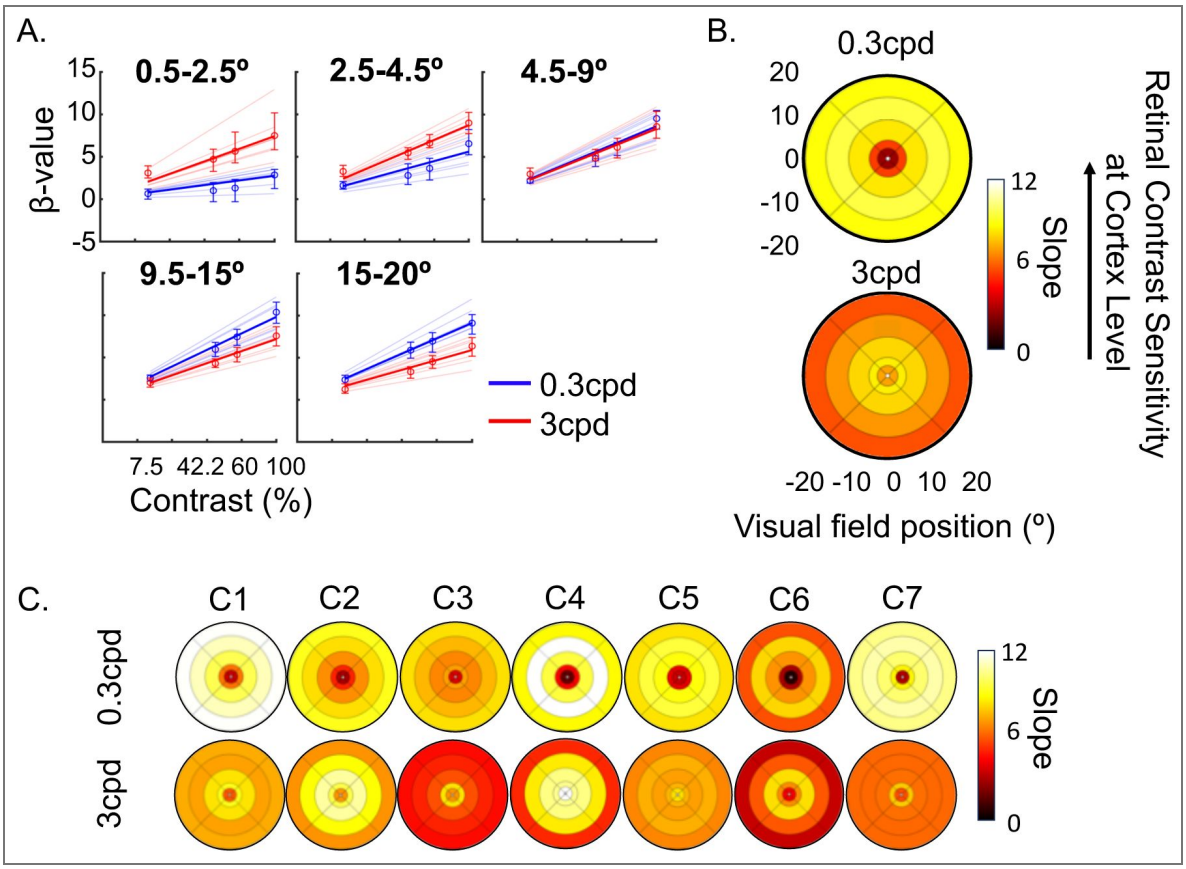

Figure 4. Spatial frequency preference V1 across the visual field.

For each participant, five eccentricity bins were defined using subject-specific pRF estimates: 0.5°-2.5°, 2.5°-4.5°, 4.5°-9.5°, 9.5°-15°, and 15°-20°. **A:** Average β-values versus stimulus contrasts for low (0.3cpd; blue) and high (3cpd; red) spatial frequencies across eccentricity bins. Error bars are the 95% confidence intervals. Thick lines represent the group-level model fit, thin lines are the individual fits. **B:** Slopes projected into visual space for low (0.3 cpd) and high (3 cpd) spatial frequencies. The color scale corresponds to slope estimates, with higher values indicating higher cortical contrast sensitivities. **C:** Heat plots for each participant (C1-C7).

the visual field (Left-Right Horizontal Meridian Anisotropy – **LRHMA:** $t(6) = 0.7197$, $p_{45,6} = 0.4988$). Moreover, there was no interaction between spatial frequency and visual field quadrant positions ($F(2.16,12.99) = 1.34$, $p = 0.298$), suggesting V1 visual field anisotropies are relatively constant across spatial frequencies. Importantly, all these differences are also present in individual participants (Figure 5A, transparent lines are individual data, Figure 5C shows individual visual field plots; for stats, see Table A2 in *Appendix* section). All participants had better V1 sensitivity in the horizontal versus vertical quadrants. 6 out of 7 participants showed asymmetries between the lower and upper quadrants. Differences in V1 sensitivity between left and right quadrants were inconsistent across participants (3 participants: left>right; 2 participants: right>left; 2 participants: non-significant), in line with no difference at the group-level. This again demonstrates the high sensitivity of our approach for identifying and quantifying sensitivity changes across the visual field, at the individual participant level, offering a potential valuable tool for assessing and addressing visual field loss in clinical populations.

We next tested if we could recover these V1 anisotropies when using retinotopic estimates based on structural scans fit with the Benson atlas instead of pRF measures (see Figure A3 and Table A3-4 in *Appendix* section). We found that the horizontal-vertical anisotropy effect was recovered (**HVA:** $t(6) = 3.584$, $p_{45,6} = 0.0347$), but that the vertical meridian anisotropy effect was not (**VMA:** $t(6) = 0.744$, $p_{45,6} = 0.9697$) with this approach. These results provide evidence that our approach can still detect subtle visual field quadrant anisotropies using a structure-based retinotopic atlas, although less accurately.

While the most pronounced contrast sensitivity difference along visual field quadrants (horizontal versus vertical quadrants) was retained when the adjusted Benson atlas was used to replace pRF measurements, not all anisotropies survived. This may be because the template does not model cortical magnification differences along meridians, reducing accuracy. It is not surprising that retinotopic estimates based on structure-retinotopy relationship modeling, provides less accurate estimates of retinotopic tuning of neuron population in V1 than direct measures of the individual retinotopy. Any individual deviations from the model make it more challenging to accurately assign cortical contrast sensitivity to visual field locations, potentially decreasing the ability to detect changes in visual function across the field. Given this challenge, results with the adjusted Benson map are surprisingly similar to those based on pRF measurement, showing promise for clinical applications when pRF mapping is unfeasible.

V1 sensitivity differences across the visual field are reproductible across visits

Having shown that changes in cortical contrast sensitivity across the visual space can be detected with fMRI, it is crucial to determine how reliable our measure is. This is especially important for potential applications in monitoring changes over time. Using Spearman correlations, we measured the reliability of cortical contrast sensitivity estimates for the 0.3cpd spatial frequency condition across two repeated measurements, collected on two different days. We collected test-retest reliability measures from 4 out of 7 participants (Figures 6A-B) and benchmarked them against the correlations between the 0.3cpd condition and 3cpd spatial frequency condition, collected in the same session (Figure 6C). If measures are reliable, correlations should be higher for repeated measures with the same spatial frequency stimulus, collected on different days. We tested this prediction using a one-tailed paired t-test. Our findings clearly show that the gradual increase in cortical sensitivity toward the periphery for the 0.3cpd condition is consistent across the two sessions (Figure 6A). Moreover, the data of individual participants show characteristic profiles that stay highly consistent. Additionally, we observed moderate-to-strong positive Spearman correlations across sessions for the 0.3cpd condition (Figure 6B; C2: $\rho = 0.5793$; C4: $\rho = 0.6996$; C5: $\rho = 0.4059$; C6: $\rho = 0.7677$), which were consistently higher than those across different spatial frequency conditions (Figure 6C; C2: $\rho = 0.5503$; C4: $\rho = 0.2318$; C5: $\rho = 0.2158$; C6: $\rho = 0.4993$). This difference was statistically significant ($t(3) = 2.62$, $p < 0.0395$). This indicates that within participants, our measure is reliable across sessions and distinguishes effectively between

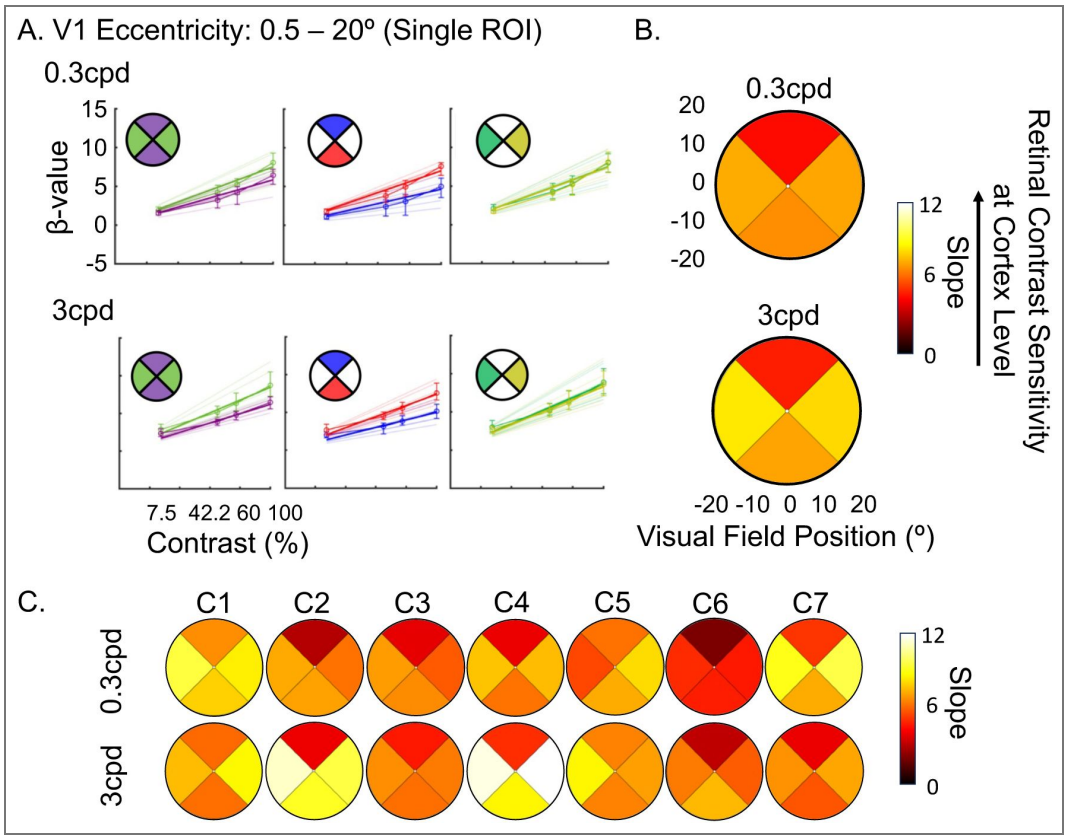

Figure 5. Anisotropies in V1 across visual field quadrants for low (0.3cpd; top row) and high (3cpd; bottom row) spatial frequencies.

pRF estimates were used to link brain responses to visual field positions. Visual quadrants are ±45° around the cardinal meridians, with slope values for eccentricities between 0.5°-20°. Horizontal quadrants are left and right; vertical quadrants are upper and lower. **A:** Average β-values versus contrast levels for each anisotropy (horizontal vs. vertical, upper vs. lower, left vs. right). Error bars are 95% confidence intervals. Thick lines correspond to average model fit, which thin lines are individual fits. **B:** Slope values projected onto visual field quadrants. The color scale represents slope estimates, with higher values indicating greater V1 contrast sensitivity. **C:** Heat plots for each participant (C1-C7).

patterns elicited by various spatial frequency conditions. Collectively, this suggests that our measure could serve as a robust tool for detecting changes in cortical sensitivity, such as those occurring over time or following therapeutic interventions.

Effect of eye movements on V1 cortical sensitivity

So far, we have demonstrated that our measure of cortical sensitivity can reliably recover known gradients in sensitivity across eccentricities and visual quadrants. We also showed that this measure was consistent across visits and sessions, suggesting its potential utility for monitoring changes over time. However, all prior tasks were conducted under conditions of central fixation, with participants instructed to maintain gaze on a central dot. A key motivation for this approach was its theoretical robustness to fixation instability. We therefore also aimed to investigate how varying degrees of eye movement might influence cortical sensitivity across the visual field.

To address this, two participants (C5 and C6) completed a modified version of the contrast sensitivity task in which they made eye movements either by following a dot moving randomly at a radius of 2° or 5° around fixation, or by self-initiated very large eye movements. Eye movements across these conditions (Figure 7, bottom row; Figure 8, bottom row), were quantified using BCEA (**C5** – Central fixation: mean±SD = 0.57±0.11 deg^2, 2° eye motion: 2.69±0.48 deg^2, 5° eye motion: 20.3±1.32 deg^2, random eye motion: 133.7±23.36 deg^2; **C6** – Central fixation: 0.96±0.56 deg^2, 2° eye motion: 1.28±0.15 deg^2). For reference, in severe (idiopathic) nystagmus, the eye movement variability along the vertical and horizontal planes is 1.08 deg and 1.60 deg, respectively (Tailor et al., 2021). Assuming a moderate correlation between axes (ρ = 0.3), the average fixation stability would equate to a BCEA of ~21.46 deg^2 (i.e., ~5° eye motion condition in our data).

Despite these very large levels of eye movements, we observed that the overall cortical contrast sensitivity spatial pattern across eccentricity remained remarkably consistent (Figure 7, top and middle rows; Figure 8, top row). However, at the most extreme movements, contrast sensitivity estimates (slope values) were lower; and while the overall cortical visual field map structure was still clearly present for low spatial frequencies, it appeared more flattened for 3cpd, suggesting reduced sensitivity of our measure for large eye movement and high spatial frequency stimuli.

A test-case of simulated loss of visual inputs

In the previous sections, we showed that the slope of a square root function provides a reliable measure of contrast sensitivity in the brain of healthy controls. But can this brain-level model also quantify loss of visual inputs? To test this, we first simulated an artificial scotoma in one normal sighted participant, by (a) masking a region of the visual field with a grey, annular ring, covering 3°-8° eccentricity (Figure 9A), and (b) masking the upper-right visual quadrant using a grey quarter-sector overlay (Figure 10A). We expect smaller slope values in V1 neuronal populations that would under normal circumstances encode that part of the visual space.

As expected, we observed reduced responses in V1 locations corresponding to the artificial scotoma (Figures 9 and 10), with increased responses along the edges of the mask for the ring scotoma condition (Figure 9B). This artificial loss of visual input was also clearly present in the cortical contrast sensitivity estimate, with significantly reduced slope steepness in V1 between 3-8° for the ring scotoma condition (Figure 9C&D) and in the upper-right quadrant for the quarter-sector scotoma condition (Figure 10B&C). Additionally, we could recover this scotoma using the calibrated Benson template, although less accurately (Figures 9E and 10D). These results show that this measure of V1 contrast sensitivity is sensitive enough to detect loss of visual inputs in the brain at an individual level, when a complete local loss of sight is simulated, and that this approach does not crucially rely on pRF mapping data from the individual. This supports the utility of our approach in recovering patterns of vision loss and recovery at a cortical level.

Case of severe central vision loss

We next tested if brain-based cortical contrast sensitivity could recover visual field loss in a clinical patient with Leber Hereditary Optic Neuropathy (LHON; M, 45.5 years old, mutation: m.11778G>A, disease duration: 36.1 years). LHON is a neurodegenerative disease caused by

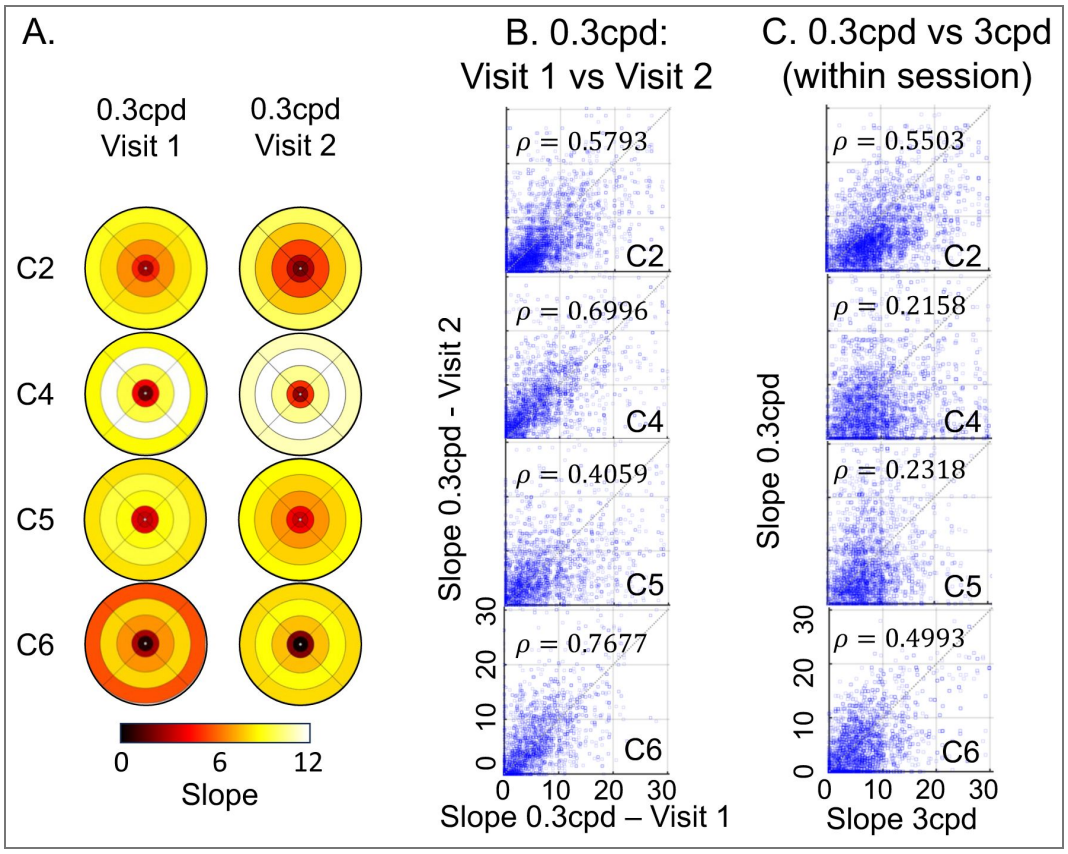

Figure 6. Reliability of V1 slopes across sessions, in 4 of the 7 controls.

A: V1 contrast sensitivity (i.e., slopes) plotted in visual field space (using pRF estimates), showing a consistent session-independent increase in cortical sensitivity toward peripheral locations for the 0.3cpd condition. Higher slopes (warmer colors) indicate higher V1 sensitivity. **B:** Slopes for the 0.3cpd condition across two visits. **C:** Slopes for the 0.3cpd and 3cpd conditions collected within the same session.

Figure 7. Effect of eye movements on slope estimation, in participant C5.

Each column represents a distinct eye movement condition: **A:** central fixation, **B:** 2° eye motion, **C:** 5° eye motion, and **D:** random eye motion. pRF estimates were used to relate brain responses to visual field positions. Top row: Heatmaps of slope distributions for low (0.3 cycles per degree, cpd) and high (3 cpd) spatial frequency stimuli, with warmer colors indicating steeper slopes . Middle row: Slope values scattered across eccentricity bins (0.5–2.5°, 2.5–4.5°, 4.5–9.5°, 9.5–15°, and 15–20°), illustrating how cortical sensitivity varies across the visual field for low (blue) and high (red) spatial frequencies. Error bars represent 95% confidence interval. Bottom row: Fixation stability plots from one out of 3 runs, including fixation points (blue) and BCEA ellipses (red). BCEA values quantify gaze dispersion: Central Fixation (0.91 deg²), 2° eye motion (2.43 deg²), 5° eye motion (18.41 deg²), and random eye motion (130.79 deg²). Despite increased eye movements and reduced slope values – particularly for high spatial frequency stimuli – the overall pattern of cortical sensitivity remains consistent across conditions.

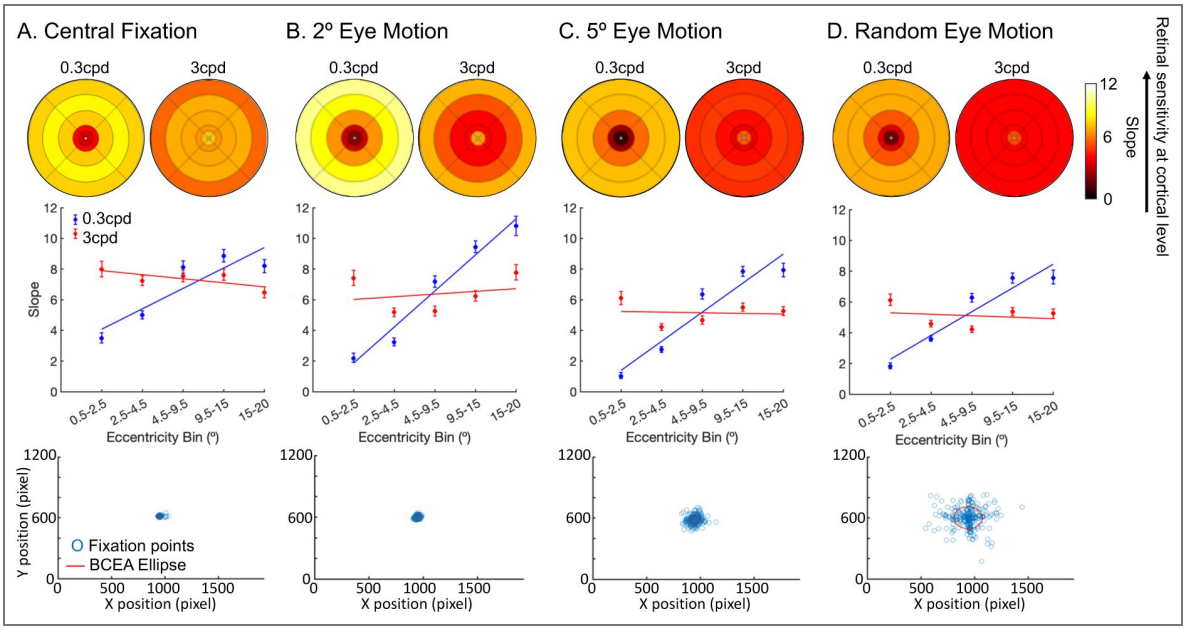

Figure 8. Effect of eye movements on slope estimation, in participant C6.

Each column represents a distinct eye movement condition, **A:** central fixation. **B:** 2° eye motion. pRF estimates were used to relate brain responses to visual field positions. Top row: Heatmaps of slope distributions for low (0.3 cycles per degree, cpd) and high (3 cpd) spatial frequency stimuli, with warmer colors indicating steeper slopes. Bottom row: Fixation stability plots from one out of 3 runs, including fixation points (blue) and BCEA ellipses (red). BCEA values quantify gaze dispersion: Central Fixation (0.76 deg²) and 2° eye motion (1.23 deg^2).

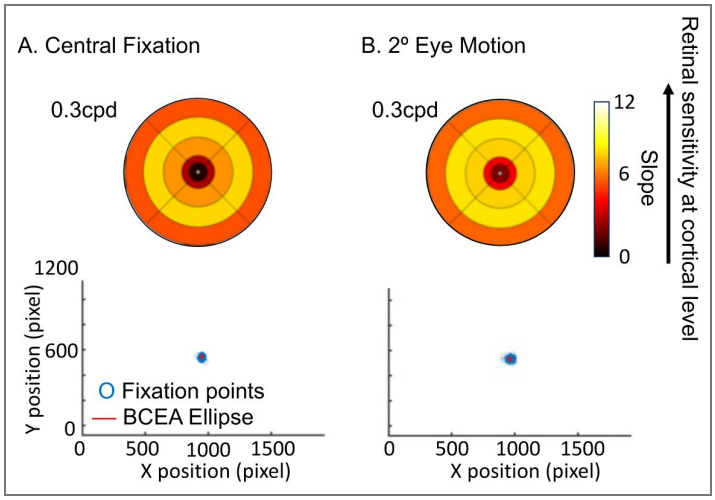

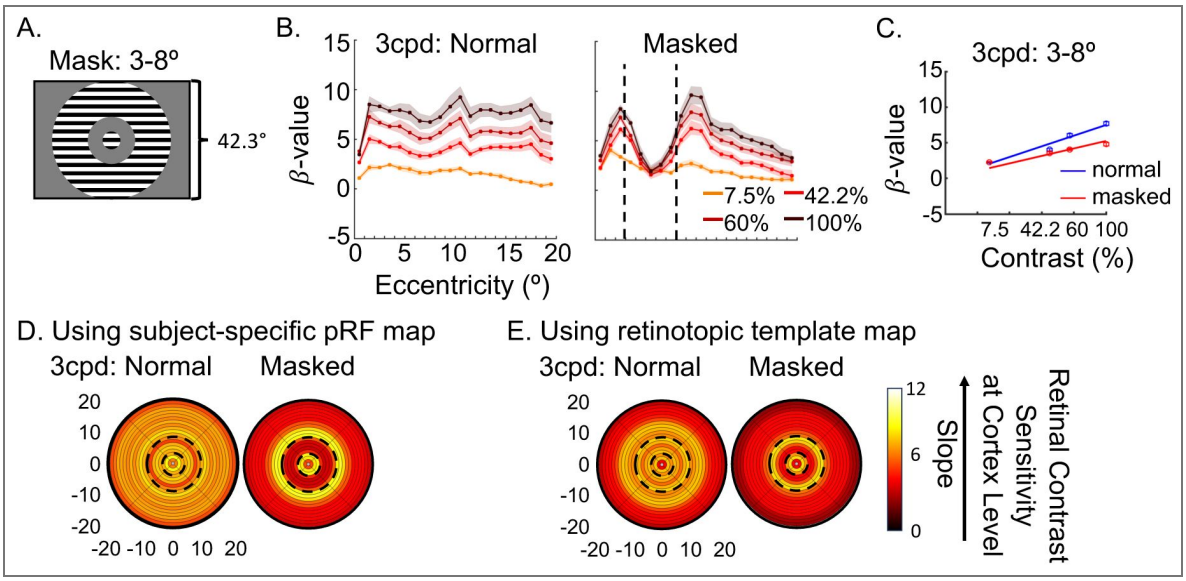

Figure 9. V1 sensitivity (i.e., slope) to 3cpd condition, in the region of the artificial scotoma (3-8°) in participant C5.

A: Masked region between 3-8°, representing the artificial scotoma. **B:** Averaged β-values between 0.5°-20° eccentricities in V1, under normal and masked conditions. 20 eccentricity bins of 1° were selected based on pRF estimates. The color scale indicates the presented contrast levels, and the black dotted lines mark the boundaries of the artificial scotoma. Shaded area represents 95% confidence interval. **C:** Average β-values versus contrast levels in V1 neurons encoding the region of artificial scotoma (3°-8°), under normal (blue) and masked (red) conditions. Lines correspond to the model fitted to the data. Error bars (masked by dots) represent 95% confidence interval. **D:** Slopes projected back onto the visual field under normal and masked conditions. pRF estimates were used to relate brain responses to visual field locations and to create the 1° eccentricity bins. The boundaries of the simulated scotoma region are represented by dotted lines. The color scale indicates slope estimates, with higher values (warmer colors) corresponding to higher V1 contrast sensitivity. **E:** Slopes plotted back into the visual space using the calibrated Benson template instead of pRF estimates.

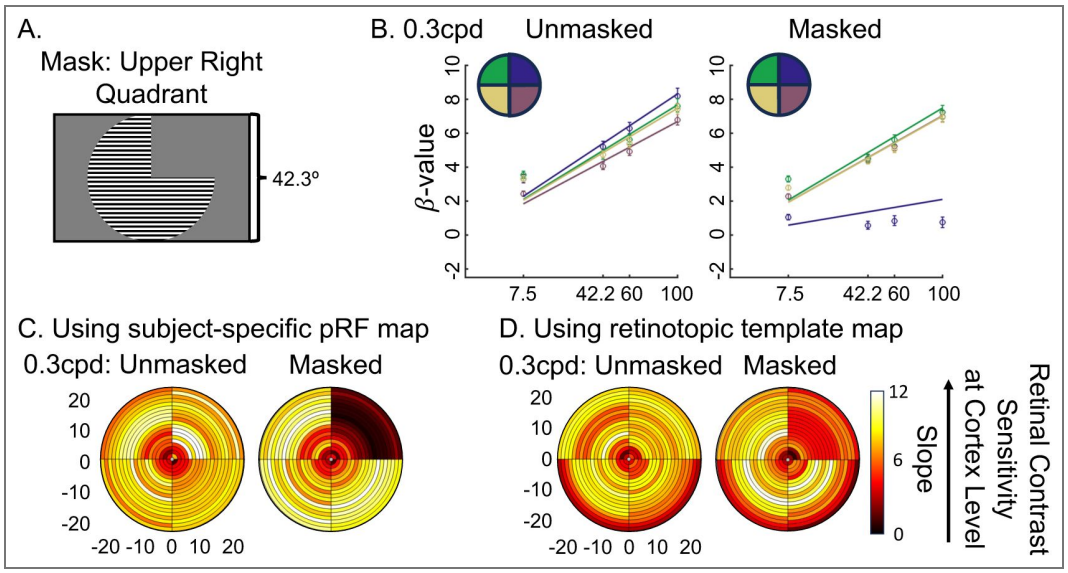

Figure 10. V1 sensitivity (i.e., slope) to 0.3cpd condition, in the region of the artificial scotoma (upper right quadrant) in participant C5.

A: Masked upper right quadrant region, representing the artificial scotoma. **B:** Average β-values versus contrast levels in V1 neurons encoding each of the four quadrants: upper left (yellow), upper right (cyan), bottom left (red), and bottom right (blue). Lines correspond to the model fitted to the data. Error bars represent 95% confidence interval. **C:** Slopes projected back onto the visual field under normal and masked conditions. pRF estimates were used to relate brain responses to visual field locations and to create the 1° eccentricity bins. The color scale indicates slope estimates, with higher values (warmer colors) corresponding to higher V1 contrast sensitivity. **D:** Slopes plotted back into the visual space using the calibrated Benson template instead of pRF estimates.

mitochondrial DNA mutations, leading to acute loss of retinal ganglion cells across large visual field areas. LHON patients often present with dense, central scotoma extending up to 10-15 degrees around fixation.

As vision loss often varies between eyes, the patient underwent monocular testing for the fMRI contrast sensitivity task (tested spatial frequencies: 0.3cpd and 1cpd). For comparison, a behavioral visual field perimetry map was obtained with the Compass fundus perimeter (CenterVue, Padova, Italy) for each eye, using a 24-2 testing grid with a Goldmann size III target (54 locations: 52 from the 24-2 grid, 1 at fixation, and 1 at the physiological blind spot). The Compass actively tracks the retina to compensate for fixation loss, automatically repositioning targets based on current eye position. Sensitivity thresholds at each location were determined using the ZEST projection strategy implemented in the device. The patient, who had some preserved central vision, could see the fixation targets in behavioral testing and the scanner, making them an ideal participant for methods evaluation.

The Compass perimetry map revealed drastic loss of sensitivity across the visual field (Figure 11 – top row). For the left eye, the left hemifield was more affected than the right, with most severe loss in the upper-left quadrant. In contrast, the right eye showed more reduced sensitivity in the right hemifield, particularly in the upper-right quadrant.

We found correspondence between affected and non-affected visual field regions across the Compass and the fMRI contrast sensitivity measures (Figure 11). Here, V1 contrast sensitivity (i.e., slope values) was computed for the upper-left, upper-right, lower-left and lower-right quadrants to match the layout from the Compass visual field maps. Using the brain-based approach, we recovered sensitivity loss in the upper-right visual quadrant for the right eye at the cortical level, reflected in smaller cortical contrast sensitivity slopes in V1 neuronal populations encoding that area. For the left eye, cortical contrast sensitivity was also lower in the upper-left quadrant of the visual field, but differences were less pronounced. This is in line with the observation that the left eye was the better eye, with substantially less severe vision loss in the affected regions (lighter shading, Figure 11 – top row). When using the calibrated Benson atlas instead of pRF mapping data to link neuronal responses to visual locations, this pattern was retained for the right eye, but the more subtle pattern in the left eye became noisier.

By combining large-field stimulation and contrast sensitivity modeling in fMRI, with the cortical magnification-adjusted Benson atlas, these data show how brain-based measures could provide a tool to characterize vision loss in patients without need for demanding tasks or sustained precise fixation, while highlighting challenges of detecting more subtle vision loss and pinpointing it to visual locations.

Discussion

In this study, we aimed to develop and validate an fMRI-based method for measuring cortical contrast sensitivity across a broad extent of the visual field in V1, addressing the limitations of traditional visual field tests and existing neuroimaging approaches. To achieve this, we implemented a large-field presentation set-up in fMRI, allowing us to stimulate the visual cortex up to 20° eccentricity. By integrating population receptive field (pRF) modeling with contrast sensitivity measurements of the BOLD response to large-field sinusoidal gratings varying in contrast levels and spatial frequencies, we created a quantitative, sensitive, and reliable measure of cortical contrast sensitivity. Our key findings demonstrate that this approach can accurately quantify known variations in V1 contrast sensitivity across eccentricity and polar angle, recover simulated and pathological visual field losses, and produce consistent and reliable measures both at the group and individual participant levels. Crucially, the ability to visualize these sensitivity gradients was made possible by the large peripheral coverage provided by our large-field stimulation set-up. Such coverage is particularly important for clinical applications, as it enables the detection of visual field losses beyond the macula (i.e., beyond 10° eccentricity) and the

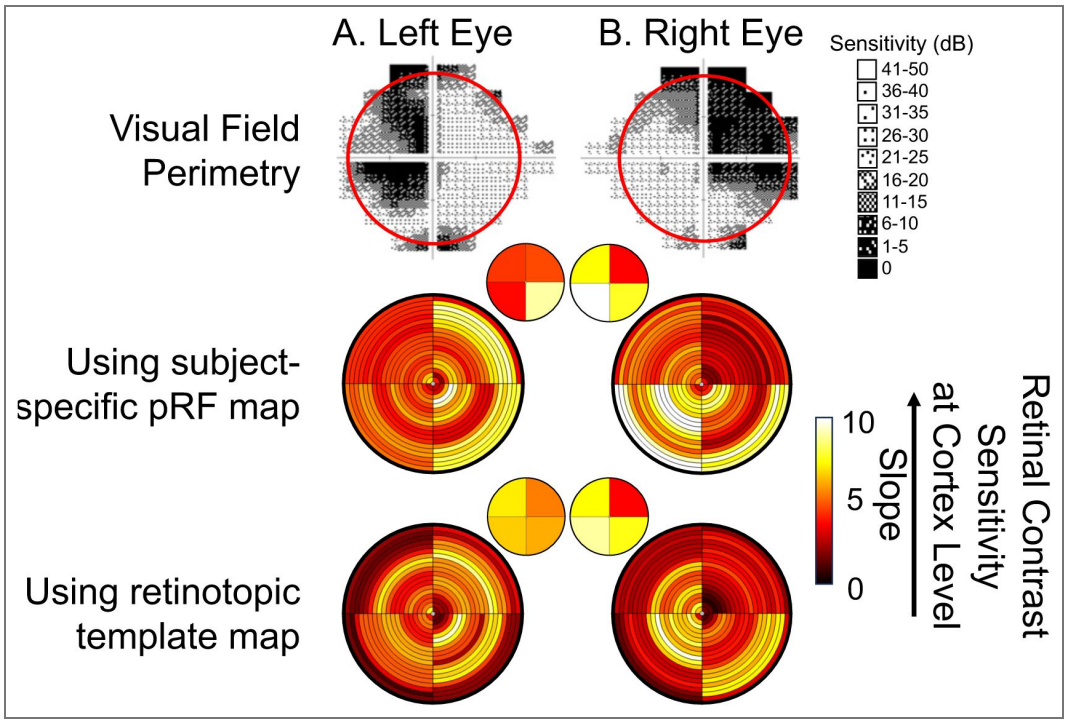

Figure 11. Correspondence between visual field perimetry map and V1 sensitivity map, in a patient with Leber Hereditary Optic Neuropathy.

A: Left eye. **B:** Right eye. **Top row:** Gray scale visual field map obtained with the Compass fundus perimeter (CenterVue, Padova, Italy), using Standard Perimetry display convention. Sensitivity is represented with symbols and related dB intervals, with larger values describing better sensitivity. Red circle indicates the area of the visual space stimulated in the fMRI contrast sensitivity task. **Middle row:** Heatmap of V1 sensitivity (i.e., slopes) across the visual field. Here, we divided the space between the upper-left, upper-right, lower-left and lower-right quadrants (as opposed to the left, right, upper and lower quadrants used in previous sections), to match the layout of visual field perimetry maps. We also only show the responses to low spatial frequency condition (0.3cpd) for visualization. Slope values were averaged for each visual quadrant and 1° eccentricity bin and projected back into the visual space, using the subject-specific pRF map. Color scale corresponds to the steepness of the slope estimate. For better visualization of sensitivity differences across quadrants, we also averaged the slopes between 0.5-20° eccentricities in each quadrant, generating a single slope value for each visual quadrant (inset heat plots). The range of slope values were reduced on the color scale for these inset plots. **Bottom row:** Heatmap of V1 sensitivity (i.e., slopes) across the visual field in response to the 0.3cpd condition, using the Benson retinotopic template map instead of the pRF data.

evaluation of residual peripheral vision in patients with macular-restricted damage. In doing so, this work provides a useful tool for advancing both basic visual neuroscience and translational research in clinical populations.

Validation of Sensitivity Variations Across the Visual Field

Our method successfully captured the expected variations in cortical contrast sensitivity across the visual field. Consistent with previous behavioral and fMRI studies (Aghajari et al., 2020; Broderick et al., 2022; D'Souza et al., 2016; Henriksson et al., 2008; Rovamo et al., 1984; Rovamo & Virsu, 1979; Welbourne et al., 2018), we observed that V1 neuronal populations encoding the central visual field exhibited higher contrast sensitivity for high spatial frequency (SF) stimuli, while those encoding peripheral regions were more sensitive to low SF stimuli. This aligns with the understanding that spatial frequency tuning varies across the visual field due to smaller pRF sizes and larger cortical areas dedicated to central vision (Himmelberg et al., 2023).

Additionally, our study identified anisotropies in contrast sensitivity across visual field quadrants, mirroring findings from previous behavioral studies (Barbot et al., 2021; Carrasco et al., 2022; Himmelberg et al., 2020). Specifically, we found enhanced cortical sensitivity in V1 neuronal populations responding to horizontal versus vertical locations and to lower versus upper visual field locations. Unlike earlier fMRI studies (Liu et al., 2006; O'Connell et al., 2016), which either could not assess horizontal-vertical effects or used smaller region selections, our use of large-field stimuli enabled the detection of both upper-lower and horizontal-vertical asymmetries. Moreover, by modeling cortical contrast sensitivity across multiple contrast levels, we were able to identify subtle variations in V1 neuron sensitivity that single-threshold approaches might overlook.

We also observed intriguing variability in cortical visual field maps across healthy controls, and this variability was consistent across measures. This may reflect genuine individual differences in visual sensitivity that are relevant for behavioral performance. Alternatively, it could arise from factors such as local signal-to-noise differences driven by anatomical variability. However, the fact that maps derived from different spatial stimulus conditions showed markedly different patterns argues against a purely anatomical explanation and suggests that at least part of the variability is functional. Despite this inter-subject variability, variations in cortical contrast sensitivity across eccentricities and visual field quadrants were significant at the individual level indicating high sensitivity.

Reliability and Sensitivity Across Sessions and Robustness to Eye Movements

We also showed that our approach was reliable over time. We found consistent activation patterns and moderate-to-high correlations in slope estimates for the 0.3cpd condition across two sessions, significantly higher than correlations across different stimuli conditions (i.e., 0.3cpd versus 3cpd). High sensitivity and reliability are essential for detecting longitudinal changes in clinical groups, such as those occurring before and after sight-rescuing interventions. Fitting a contrast response function to the BOLD signal might offer robust estimates of visual function by minimizing the impacts of overall BOLD amplitude variability and arbitrary thresholds.

Crucially, one advantage of cortical visual field mapping is that the maps are inherently centered on the foveal confluence, providing a stable reference point for comparing responses across eccentricities. When combined with large-field, spatially homogeneous stimuli, this anchoring means that our approach should remain robust to moderate fixation variability and still quantify sensitivity changes across the visual field – provided that fixation instability does not exceed the stimulus extent (40° diameter).

When measuring the impact of eye movements, we found that spatial sensitivity patterns were largely preserved, even for extreme eye movements (emulating severe nystagmus). However, under the most extreme conditions, sensitivity estimates (i.e., slope values) were reduced, especially for high spatial frequency (SF) stimuli. This likely reflects image blurring from large

rapid eye movements, which degrades high-SF inputs and shifts activation toward neurons tuned to lower SFs. This aligns with evidence that nystagmus and large saccades impair perception of fine detail and grating stimuli due to retinal image slip (Abadi & Bjerre, 2002; Dickinson & Abadi, 1985; Hertle et al., 2017; Randall et al., 2020). While classic findings report suppression of low-SF signals during saccades (Burr et al., 1994; Ross et al., 2001), our results suggest that high SF sensitivity may be more vulnerable to large eye movements when participants are presented with 2Hz phase-flickering gratings. Further validation in clinical groups with naturally-occurring fixation instability would further strengthen these conclusions.

Mapping Simulated and Pathology-Driven Vision Loss

Our method successfully identified both simulated retinal loss in a healthy volunteer and real visual field loss in a patient with Leber Hereditary Optic Neuropathy (LHON). The signal drop observed in response to masking portions of the visual field in the healthy control was both large and significant at the individual level, as demonstrated by non-overlapping 95% confidence intervals (Figures 9B-C and 10B). This provides proof-of-concept evidence that our approach can detect signal changes in individual patients, which is a critical requirement for clinical translation.

Unlike previous fMRI studies that used high-contrast stimuli (Farahbakhsh et al., 2022; Pawloff et al., 2023; Ritter et al., 2019), which may not accurately represent partial vision loss due to potential saturation effects and the stimulation of less sensitive retinal cells, our use of multiple contrast levels offers a more nuanced assessment of cortical contrast sensitivity. Combined with the large-field set-up allowing stimulation up to 20° eccentricity, this approach may be particularly well-suited for evaluating treatment efficacy in cases of widespread and variable vision loss.

Future work will focus on further validating reconstruction accuracy under controlled conditions, including simulated scotomas of varying severity and location, expanding testing to larger patient cohorts, and establishing a normative dataset to contextualize patient data.

Limitations of pRF Mapping, Advances in Structure-Based Templates, and Future Directions in Brain-Based Visual Field Mapping

One limitation of this brain-based approach to visual field testing, is its reliance on pRF mapping, which requires precise fixation and can be challenging to acquire in visually impaired patients. To mitigate this, we investigated the use of retinotopic templates based on anatomical landmarks (Benson et al., 2014; Benson & Winawer, 2018), thereby reducing the need for pRF data collection and facilitating the mapping of brain responses to visual field positions. Particularly at large eccentricities however, we initially observed inaccuracies between the template and individual retinotopy eccentricity estimates which led to substantial distortions in cortical visual field maps due to cortical magnification (see Figure A4 in *Appendix* section). To address this, we adjusted the Benson eccentricity estimates to align with the cortical magnification scaling function (Horton & Hoyt, 1991).

With this structure-based atlas, we successfully replicated key variations in visual field function (across eccentricity and polar quadrants), although sensitivity to more subtle differences (e.g., upper versus lower quadrant anisotropy) was reduced. This reduction may partly stem from differences in ROI definitions: a manually delineated V1 mask was used for the pRF-based data, while the Benson atlas mask was used for the adjusted Benson atlas analysis. Such differences could introduce minor error beyond the atlas/pRF mapping itself due to differences in the vertices included by each mask.

Beyond ROI considerations, we still observed differences in cortical sensitivity between pRF mapping and the adjusted Benson atlas – particularly in the periphery. Several factors likely contribute to this. First, individual differences in the relationship between cortical structure and retinotopy are not fully captured by the template. Second, the Benson atlas has never been fit with empirical data more eccentric than approximately 20°, which naturally limits its precision in the far periphery. Third, because of cortical magnification, any small inaccuracy at larger

eccentricities has a disproportionately large effect, making peripheral vertices more susceptible to mis-assignment than central ones. These influences introduce systematic distortions in cortical visual field maps rather than random noise and thus remain consistent across timepoints – an important point when assessing longitudinal changes (e.g., ageing or gene-therapy interventions). Importantly, the spatial gradients in cortical contrast sensitivity were preserved across both the pRF and Benson atlas approaches, indicating that minor ROI differences do not affect our conclusions. Together, these findings show that the Benson atlas remains a useful alternative when pRF mapping is not feasible.

It is also promising that cortical structure-based templates can successfully recover visual field loss through simulation or the neurodegenerative disease LHON. Critically, in patient groups with severe impairment such as LHON, where it is often very challenging or impossible to obtain reliable measures, even imperfect mapping between the brain and visual field could offer important improvements over available solutions for tracking functional change, and where they stem from. Further enhancing the alignment between retinotopic template atlases and individual retinotopic tuning could improve this approach further, for example, by integrating them with functional measures using Bayesian methods (Benson & Winawer, 2018). In parallel, geometric deep learning frameworks such as DeepRetinotopy (Ribeiro et al., 2021) could also offer anatomy-driven predictions from structural MRI, and combining these strategies may yield more accurate and generalizable retinotopic reconstructions.

While our method demonstrated high accuracy and reliability in sighted controls, further validation in patients is necessary to ensure the generalizability of our approach to measuring pathology. Next steps in this work will therefore involve testing larger patient cohorts with diverse forms of vision loss, validating the approach for tracking pathology over time, and investigating how cortex-based visual field measures relate to and complement other visual field and retinal integrity indices including Compass measures and OCT-derived retinal layer thickness. For example, while we reasoned that using a single high contrast stimulus is likely to give less reliable measures for various reasons outlined above, this needs to be tested empirically. It also remains unclear whether the square root contrast response function is optimal for patients, who are likely to show different non-linearities in their contrast response. In addition, comparing the cortical contrast sensitivity modeling approach presented here with alternative framework (e.g., neural contrast sensitivity functions proposed by Roelofzen et al., 2025) will be another interesting direction for future research. Finally, more extensive mapping of the spatial frequency and contrast sensitivity spaces could offer additional informative measures such as cortical acuity and spatial frequency preferences, provided such measures are feasible with patient-friendly protocols.

Conclusion

In sum, brain-based contrast sensitivity measures could significantly enhance the accurate characterization of visual field function in blinding diseases, by addressing limitations of traditional visual field tests that are subjective, time-consuming, and challenging for patients with severe sight loss. By providing a reliable, quantitative measure of cortical contrast sensitivity across the visual field, fMRI may help facilitate the monitoring of disease progression and recovery, including interventions like gene therapy. Combined with our large-field stimulation setup and fixation free approaches to linking cortical sensitivity estimates to visual field locations, this method is well-suited for a wide range of visual impairments, addressing a pressing challenge in the evaluation of current clinical trials. Additionally, linking brain-based variations in function across the visual field to behavioral performance (e.g., perimetry, microperimetry) and retinal structure (fundus imaging, retinal thickness from Optical Coherence Tomography), could help bridge the gap between neural measures and functional outcomes. Such integration would provide deeper insights into developmental, learning, and vision loss mechanisms.

In conclusion, integrating cortical contrast sensitivity testing with large-field stimulation and a calibrated retinotopic atlas provides a promising tool for characterizing visual field impairments, and could offer a valuable addition to existing measures of visual field loss.

Data availability

All post-processed and anonymised data are available on Zenodo (*https://doi.org/10.5281/zenodo.19051439*). Codes to reproduce the figures from the provided dataset are available on GitHub (*https://github.com/HugoCWB/ChowWingBomEtAl_2025_eLife*). Codes to adjust the Benson maps eccentricity is available on GitHub (*https://github.com/HugoCWB/AdjustEccTool*). A Docker image for the Benson eccentricity adjustment toolbox is also available on Zenodo (*https://doi.org/10.5281/zenodo.18770065*). For any queries or raw data requests, please email the corresponding author (hugo.chow-wing-bom.15@ucl.ac.uk).

Acknowledgements

This work was funded by Moorfields Eye Charity PhD Studentship GR001315 (London, UK), the Wellcome Career Development Award (306332/Z/23/Z; London, UK), and the Birkbeck-UCL Centre for NeuroImaging (BUCNI; London, UK). PYWM is supported by an Advanced Fellowship Award (NIHR301696) from the UK National Institute of Health Research (NIHR). PYWM also receives funding from Fight for Sight (UK), the Isaac Newton Trust (UK), Moorfields Eye Charity (GR001376), the Addenbrooke's Charitable Trust, the National Eye Research Centre (UK), the International Foundation for Optic Nerve Disease (IFOND), the NIHR as part of the Rare Diseases Translational Research Collaboration, the NIHR Cambridge Biomedical Research Centre (NIHR203312), and the NIHR Biomedical Research Centre based at Moorfields Eye Hospital NHS Foundation Trust and UCL Institute of Ophthalmology (NIHR203322). The views expressed are those of the author(s) and not necessarily those of the NHS, the NIHR or the Department of Health. We extend our thanks to Simon Richardson and Oliver Josephs for their assistance in the design and conception of the large-field set-up.

Appendix

A. Large-Field set-up

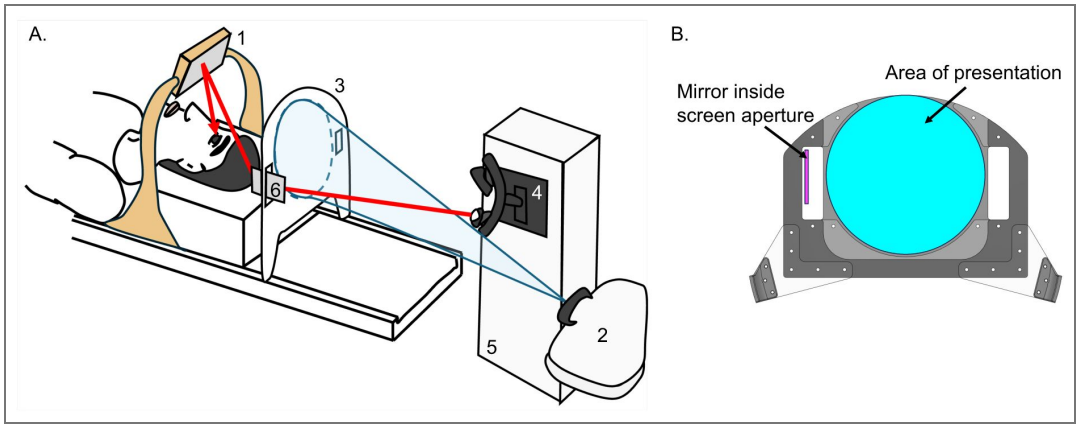

Figure A1. Schematic of Large-Field Set-Up. A: The participant lies on the scanner bed in the 64-channel coil without top to reduce obstruction and views the 40° screen via a mirror above their face (1). Stimuli are displayed using back-projection from a projector (2) outside the room, onto a screen (3) positioned behind the participant's head. The top of the screen follows the scanner bore curvature to maximize field of view. Monocular eye-tracking is achieved by mounting the illuminator and camera of the eye-tracker (4) vertically on a support (5) at the back of the scanner bore. An image of the eye is obtained via a dual-mirror set-up, including a small mirror inside an aperture cut on the side of the screen (6) and the participant mirror (1). If the right eye is being tracked, the eye-tracker is placed on the left side of the scanner bore, and the eye-tracker mirror (6) is placed in the right screen

aperture. **B:** Schematic of the large-field screen, with the area of stimulus presentation shown in cyan and the mirror used for eye-tracking in magenta. The mirror is positioned within one of the two rectangular apertures cut on either side of the screen.

B. Individual Level

To test for contrast sensitivity differences across the visual field in individual participants, we also employed a multilevel modeling approach using the lme4 package in R (Bates et al., 2015; R Core Team, 2023). This approach reduces the impact of vertex-level variability and redundancy. The model included the square root of stimulus contrast as a continuous fixed-effect predictor, and eccentricity, polar location, and spatial frequency as categorical fixed-effect predictors, along with all possible interactions. Again, the intercept was fixed at 0. The model also included random slopes for the square root contrast and the interaction between square root contrast and voxel-specific factors and was fit separately for each participant. In the formula notation used in the R package lme4, the model would be defined as:

$$\beta \sim 0$$

SubID	Effects	*Df*	Sum Sq	Mean Sq	*F*-value	*Pr*(>*F*)	Signif.
C1	SF	1	3720	3720	72.49	< 2e-16	***
	Eccentricity	1	35003	35003	681.995	< 2e-16	***
	PolarLocation	3	11258	3753	73.115	< 2e-16	***
	SF:Eccentricity	1	23914	23914	465.938	< 2e-16	***
	SF:PolarLocation	3	1546	515	10.041	1.32E-06	***
	Eccentricity:PolarLocation	3	200	67	1.297	0.274	
	SF:Eccentricity:PolarLocation	3	1158	386	7.519	5.04E-05	***
	Residuals	12378	635290	51			
C2	SF	1	23704	23704	743.628	< 2e-16	***
	Eccentricity	1	13503	13503	423.609	< 2e-16	***
	PolarLocation	3	46442	15481	485.647	< 2e-16	***
	SF:Eccentricity	1	10587	10587	332.135	< 2e-16	***
	SF:PolarLocation	3	2981	994	31.169	< 2e-16	***
	Eccentricity:PolarLocation	3	2881	960	30.126	< 2e-16	***
	SF:Eccentricity:PolarLocation	3	373	124	3.899	8.52E-03	**
	Residuals	11604	369897	32			
C3	SF	1	27	27	1.374	0.2411	
	Eccentricity	1	578	578	29.019	7.33E-08	***
	PolarLocation	3	7315	2438	122.52	< 2e-16	***
	SF:Eccentricity	1	14719	14719	739.59	< 2e-16	***
	SF:PolarLocation	3	257	86	4.311	4.80E-03	**

	Eccentricity:PolarLocation	3	2225	742	37.261	< 2e-16	***
	SF:Eccentricity:PolarLocation	3	510	170	8.543	1.16E-05	***
	Residuals	9860	196225	20			
C4	SF	1	25290	25290	521.73	< 2e-16	***
	Eccentricity	1	3970	3970	81.89	< 2e-16	***
	PolarLocation	3	34475	11492	237.08	< 2e-16	***
	SF:Eccentricity	1	75054	75054	1548.38	< 2e-16	***
	SF:PolarLocation	3	2514	838	17.29	3.40E-11	***
	Eccentricity:PolarLocation	3	16417	5472	112.89	< 2e-16	***
	SF:Eccentricity:PolarLocation	3	3921	1307	26.97	< 2e-16	***
	Residuals	9896	479688	48			
C5	SF	1	554	554	16.332	5.37E-05	***
	Eccentricity	1	6717	6717	198.161	< 2e-16	***
	PolarLocation	3	886	295	8.711	9.12E-06	***
	SF:Eccentricity	1	13436	13436	396.384	< 2e-16	***
	SF:PolarLocation	3	4753	1584	46.744	< 2e-16	***
	Eccentricity:PolarLocation	3	3023	1008	29.727	< 2e-16	***
	SF:Eccentricity:PolarLocation	3	2638	879	25.939	< 2e-16	***
	Residuals	7728	261956	34			
C6	SF	1	6008	6008	246.099	< 2e-16	***
	Eccentricity	1	21371	21371	875.448	< 2e-16	***
	PolarLocation	3	11850	3950	161.806	< 2e-16	***
	SF:Eccentricity	1	12327	12327	504.98	< 2e-16	***
	SF:PolarLocation	3	714	238	9.745	2.04E-06	***
	Eccentricity:PolarLocation	3	1569	523	21.425	7.97E-14	***
	SF:Eccentricity:PolarLocation	3	762	254	10.409	7.80E-07	***
	Residuals	9360	228493	24			
C7	SF	1	10703	10703	278.799	< 2e-16	***
	Eccentricity	1	19431	19431	506.149	< 2e-16	***
	PolarLocation	3	18754	6251	162.84	< 2e-16	***
	SF:Eccentricity	1	19611	19611	510.822	< 2e-16	***
	SF:PolarLocation	3	153	51	1.325	2.64E-01	
	Eccentricity:PolarLocation	3	12080	4027	104.885	< 2e-16	***
	SF:Eccentricity:PolarLocation	3	1380	460	11.983	7.90E-08	***
	Residuals	10794	414384	38			
Signif. codes: 0 '***' 0.001 '**' 0.01 '*' 0.05 '.' 0.1 ' ' 1							

Table A1. Results from the multilevel modelling approach in each individual participant. pRF mapping was used to link brain responses to visual field locations.

SubID	Effects	*contrast*	estimate	SE	df	t.ratio	p.value	
C1	PolarLocation	HM>VM	5.5138156	0.3278444	12354	16.818391	8.917786e-63	***
		LVM>UVM	0.5999187	0.2796053	12354	2.145591	0.03192504	*
		LHM>RHM	0.7058217	0.1711807	12354	4.123254	3.759997e-05	***
C2	PolarLocation	HM>VM	5.533751	0.2284595	11580	24.22203	1.771783e-126	***
		LVM>UVM	4.387544	0.1852974	11580	23.67839	4.420105e-121	***
		LHM>RHM	2.288693	0.1336361	11580	17.12630	5.942464e-65	***
C3	PolarLocation	HM>VM	3.568024	0.2172194	9836	16.425896	7.786414e-60	***
		LVM>UVM	2.317875	0.1801032	9836	12.869704	1.339442e-37	***
		LHM>RHM	0.159411	0.1214377	9836	1.312697	0.1893155	
C4	PolarLocation	HM>VM	7.3408010	0.3070954	9872	23.903972	8.223761e-123	***
		LVM>UVM	3.1514598	0.2492052	9872	12.646043	2.250910e-36	***
		LHM>RHM	-0.9417519	0.1794558	9872	-5.247821	1.571031e-07	***
C5	PolarLocation	HM>VM	2.2997460	0.2874033	7704	8.001807	1.405261e-15	***
		LVM>UVM	0.2736311	0.2296279	7704	1.191628	0.2334437	
		LHM>RHM	-0.2201730	0.1728344	7704	-1.273896	0.2027387	
C6	PolarLocation	HM>VM	1.8040008	0.2259007	9336	7.985813	1.561107e-15	***
		LVM>UVM	3.2006411	0.1818476	9336	17.600678	3.057311e-68	***
		LHM>RHM	0.3046082	0.1340245	9336	2.272779	0.02306211	*
C7	PolarLocation	HM>VM	5.9085493	0.3067623	10770	19.261005	2.637528e-81	***
		LVM>UVM	2.0334164	0.2617710	10770	7.767922	8.703410e-15	***
		LHM>RHM	-0.3370417	0.1599345	10770	-2.107373	0.03510831	*
Signif. codes: 0 '***' 0.001 '**' 0.01 '*' 0.05 '.' 0.1 ' ' 1								

Table A2. Post-Hoc test on ANOVA visual quadrant position effect (PolarLocation) at the individual level. pRF mapping was used to relate brain responses to visual field locations.

C. Calibrated Benson Template

Measure of Interest: Slope	num Df	den Df	MSE	F	ges	Pr(>F)	
SF	1.0000	6.0000	31.436	0.6117	0.010887	0.4639018	
ECC	2.1650	12.9901	32.694	4.7020	0.160027	0.0270342	*
PolarLocation	1.7729	10.6374	27.316	7.0357	0.163209	0.0129521	*
SF:Eccentricity	2.2706	13.6238	7.438	29.4822	0.221807	7.552e-06	***
SF:PolarLocation	1.5885	9.5309	5.173	2.1025	0.009793	0.1783533	
Eccentricity: PolarLocation	12.0000	72.0000	5.253	2.9645	0.096634	0.0020990	**
SF: Eccentricity: PolarLocation	12.0000	72.0000	1.195	3.5212	0.028091	0.0003995	***
Signif. codes: 0 '***' 0.001 '**' 0.01 '*' 0.05 '.' 0.1 ' ' 1							

Table A3. Group-Level ANOVA analysis on slope estimates, as function of spatial frequency, eccentricities, and visual quadrant positions. The Benson template retinotopic map was used to relate brain responses to visual field locations.

Measure of Interest: Slope	contrast	estimate	SE	df	t.ratio	p.value
PolarLocation	Horizontal>Vertical	4.3378240	1.2101752	6	3.5844596	0.01158079
	Lower>Upper	0.5249520	0.7053736	6	0.7442184	0.48485944
	Left>Right	-0.2265194	0.3922638	6	-0.5774671	0.58462631
SF:Eccentricity	3cpd-0.3cpd: 0.5-2.5º	4.5917619	0.7960846	6	5.7679320	0.001185113
	3cpd-0.3cpd: 2.5-4.5º	2.5801243	1.0192745	6	2.5313340	0.044599322
	3cpd-0.3cpd: 4.5-9.5º	-0.2927635	0.9981812	6	-0.2932969	0.779175269
	3cpd-0.3cpd: 9.5-15º	-1.9782789	0.6042727	6	-3.2738182	0.016953076
	3cpd-0.3cpd: 15-20º	-2.2803080	0.6462658	6	-3.5284368	0.012391168

Table A4. Post-hoc t-test analysis for the visual quadrant position effect (PolarLocation) and the interaction between spatial frequency and eccentricities (SF:Eccentricity) reported in Table A3. The Benson template retinotopic map was used to relate brain responses to visual field locations.

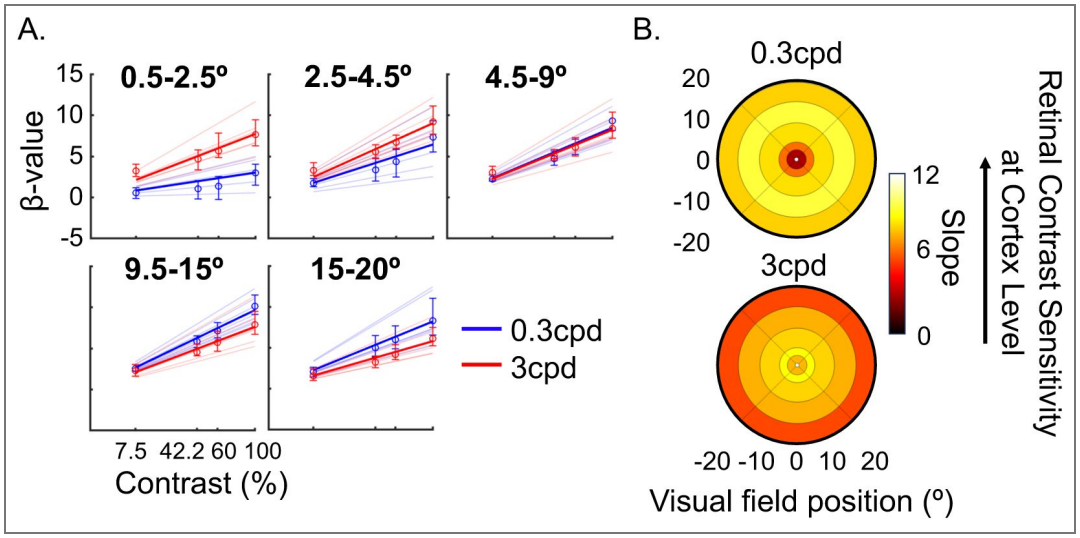

Figure A2. V1 contrast sensitivity (i.e., slopes) across 5 eccentricity bins (0.5°-2.5°, 2.5°-4.5°, 4.5°-9.5°, 9.5°-15°, and 15-20°), defined using the calibrated Benson atlas. A: β-values versus contrast levels for each eccentricity bin. Blue and red lines represent the contrast sensitivity model fits for the 0.3cpd and 3cpd conditions, respectively. Thinner lines correspond to individual fits. **B:** V1 contrast sensitivity index (i.e., slope) projected back into the visual space using the calibrated Benson atlas, for each eccentricity bin and spatial frequency condition. The color scale indicates slope estimates, with higher values representing higher V1 contrast sensitivity.

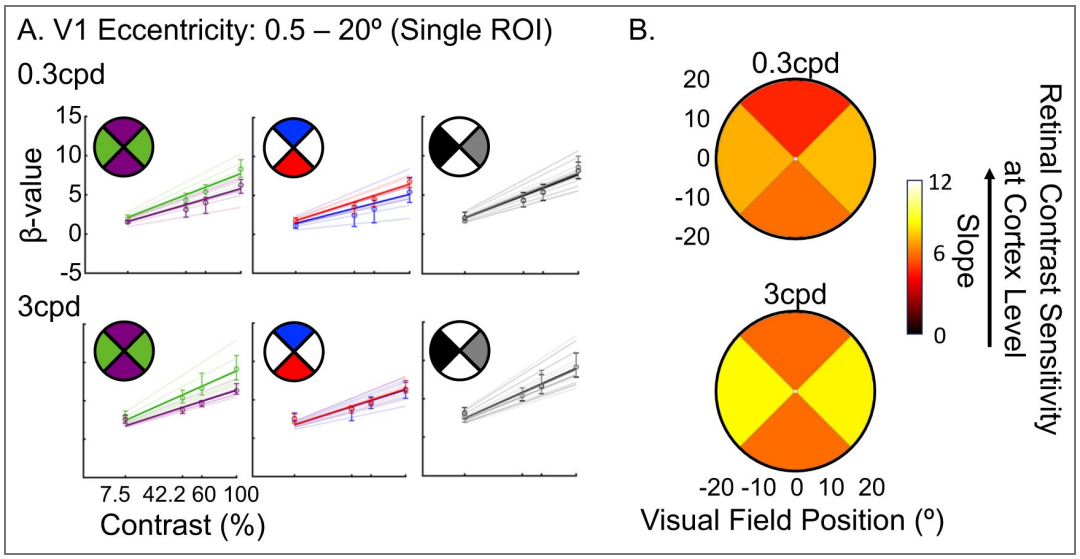

Figure A3. V1 contrast sensitivity (i.e., slopes) across visual field quadrants using the calibrated Benson atlas, for the 0.3cpd and 3cpd conditions. Visual quadrants were defined as ±45° regions around the cardinal meridians and slope values were selected for eccentricities between 0.5-20°. Horizontal quadrants are left and right, whilst upper and lower quadrants define the vertical quadrants. **A:** β-values versus contrast levels for each anisotropy effects: horizontal versus vertical, upper versus lower, and left versus right. Group-level model fits are in thick lines, whilst thinner lines correspond to individual fits. Error bars represent the 95% confidence intervals. **B:** V1 contrast sensitivity index (i.e., slope) projected back into the upper, lower, left and right visual field quadrants for the 0.3cpd and 3cpd conditions. The color scale represents slope estimates, with higher values indicating higher V1 contrast sensitivity.

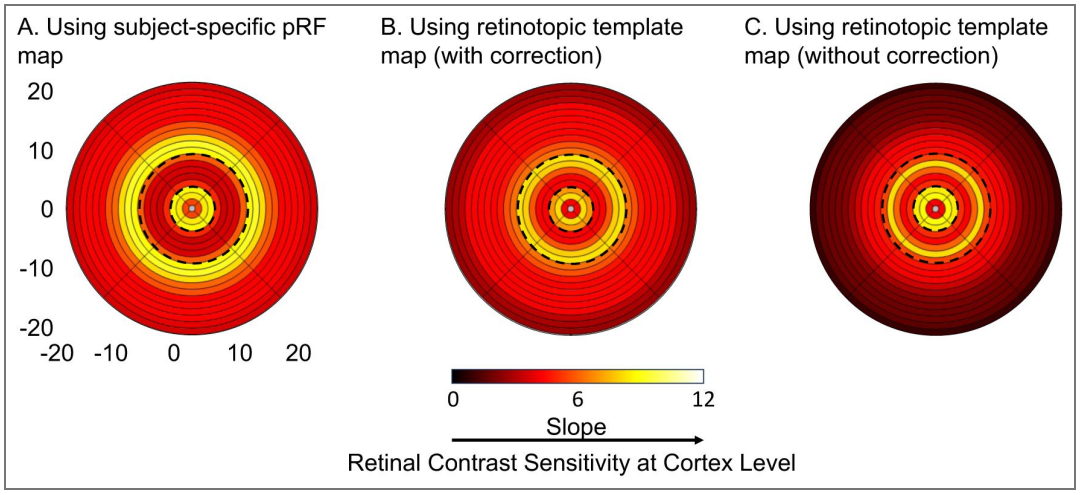

Figure A4. Effect of correcting eccentricity distribution in retinotopic templates on cortical contrast sensitivity maps. Heatmaps show slope values back projected into visual space, with each concentric circle representing a 1° eccentricity bin. **A:** Back projection was performed using subject-specific pRF map, **B:** Using Benson atlas with eccentricity distribution corrected using the H&H model. **C:** Using Benson atlas without correction (original template). Color scale indicates slope values reflecting cortical contrast sensitivity (brighter = larger slopes).

Additional information

Funding

Funder	Grant reference number	Author
Moorfields Eye Charity	PhD Studentship GR001315	Tessa Dekker
Wellcome Trust	https://doi.org/10.35802/306332	Tessa Dekker
Birkbeck-UCL Centre for NeuroImaging, London, UK		Tessa Dekker Hugo T Chow-Wing-Bom

Author ORCID iDs

Hugo T Chow-Wing-Bom: https://orcid.org/0000-0003-3348-3005
Noah C Benson: https://orcid.org/0000-0002-2365-8265
Frederic Dick: https://orcid.org/0000-0002-2933-3912
Roni O Maimon-Mor: https://orcid.org/0000-0001-5262-9976
Tessa M Dekker: https://orcid.org/0000-0002-3616-2859

Author notes

Funding: This work was funded by Moorfields Eye Charity PhD Studentship GR001315 (London, UK), the Birkbeck-UCL Centre for NeuroImaging (BUCNI; London, UK); and Wellcome Career Development Award (306332/Z/23/Z). The funders had no role in study design, data collection and analysis, decision to publish, or preparation of the manuscript.
Commercial Relationships: None
Competing interests: No competing interests declared

References

1. **Abadi R V,** Bjerre (2002) Motor and sensory characteristics of infantile nystagmus. *British Journal of Ophthalmology* **86**:1152-1160 https://doi.org/10.1136/bjo.86.10.1152 | PubMed
2. **Aghajari S,** Vinke L N, Ling S (2020) Population spatial frequency tuning in human early visual cortex. *Journal of Neurophysiology* **123**:773-785 https://doi.org/10.1152/jn.00291.2019 | PubMed
3. **Alvarez G A** (2011) Representing multiple objects as an ensemble enhances visual cognition. *Trends in Cognitive Sciences* **15**:122-131 https://doi.org/10.1016/j.tics.2011.01.003 | PubMed
4. **Barbot A,** Xue S, Carrasco M (2021) Asymmetries in visual acuity around the visual field. *Journal of Vision* **21**:1-23 https://doi.org/10.1167/JOV.21.1.2 | PubMed
5. **Bates D,** Mächler M, Bolker B, Walker S (2015) Fitting Linear Mixed-Effects Models Using **lme4**. *Journal of Statistical Software* **67**:v067i01 https://doi.org/10.18637/jss.v067.i01
6. **Benson N C,** Butt O H, Brainard D H, Aguirre G K (2014) Correction of Distortion in Flattened Representations of the Cortical Surface Allows Prediction of V1-V3 Functional Organization from Anatomy. *PLoS Computational Biology* **10**:e1003538 https://doi.org/10.1371/journal.pcbi.1003538 | PubMed
7. **Benson N C,** Winawer J (2018) Bayesian analysis of retinotopic maps. *eLife* **7**:e40224 https://doi.org/10.7554/eLife.40224 | PubMed
8. **Bourne R,** Steinmetz J D, Flaxman S, Briant P S, Taylor H R, Resnikoff S, Casson R J, Abdoli A, Abu-Gharbieh E, Afshin A, *et al.* (2021) Trends in prevalence of blindness and distance and near vision impairment over 30 years: An analysis for the Global Burden of Disease Study. *The Lancet Global Health* **9**:e130-e143 https://doi.org/10.1016/S2214-109X(20)30425-3 | PubMed
9. **Broderick W F,** Simoncelli E P, Winawer J (2022) Mapping spatial frequency preferences across human primary visual cortex. *Journal of Vision* **22**:1-21 https://doi.org/10.1167/jov.22.4.3 | PubMed

10. **Buracas G T,** Boynton G M (2007) The effect of spatial attention on contrast response functions in human visual cortex. *Journal of Neuroscience* **27**:93-97 https://doi.org/10.1523/JNEUROSCI.3162-06.2007 | PubMed

11. **Buracas G T,** Fine I, Boynton G M (2005) The relationship between task performance and functional magnetic resonance imaging response. *Journal of Neuroscience* **25**:3023-3031 https://doi.org/10.1523/JNEUROSCI.4476-04.2005 | PubMed

12. **Burr D C,** Morrone M C, Ross J (1994) Selective suppression of the magnocellular visual pathway during saccadic eye movements. *Nature* **371**:511-513 https://doi.org/10.1038/371511a0 | PubMed

13. **Carrasco M,** Roberts M, Myers C, Shukla L (2022) Visual field asymmetries vary between children and adults. *Current Biology* **32**:R509-R510 https://doi.org/10.1016/j.cub.2022.04.052 | PubMed

14. **Cauley S F,** Polimeni J R, Bhat H, Wald L L, Setsompop K (2014) Interslice leakage artifact reduction technique for simultaneous multislice acquisitions: Interslice Leakage Artifact Reduction Technique. *Magnetic Resonance in Medicine* **72**:93-102 https://doi.org/10.1002/mrm.24898 | PubMed

15. **DeYoe E A,** Carman G J, Bandettini P, Glickman S, Wieser J, Cox R, Miller D, Neitz J (1996) Mapping striate and extrastriate visual areas in human cerebral cortex. *Proceedings of the National Academy of Sciences* **93**:2382-2386 https://doi.org/10.1073/pnas.93.6.2382 | PubMed

16. **Dickinson C M,** Abadi R V (1985) The influence of nystagmoid oscillation on contrast sensitivity in normal observers. *Vision Research* **25**:1089-1096 https://doi.org/10.1016/0042-6989(85)90097-5 | PubMed

17. **D'Souza D V,** Auer T, Frahm J, Strasburger H, Lee B B (2016) Dependence of chromatic responses in V1 on visual field eccentricity and spatial frequency: An fMRI study. *Journal of the Optical Society of America A* **33**:A53 https://doi.org/10.1364/JOSAA.33.000A53 | PubMed

18. **Dumoulin S O,** Wandell B A (2008) Population receptive field estimates in human visual cortex. *NeuroImage* **39**:647-660 https://doi.org/10.1016/j.neuroimage.2007.09.034 | PubMed

19. **Engel S** (1997) Retinotopic organization in human visual cortex and the spatial precision of functional MRI. *Cerebral Cortex* **7**:181-192 https://doi.org/10.1093/cercor/7.2.181 | PubMed

20. **Farahbakhsh M,** Anderson E J, Maimon-Mor R O, Rider A, Greenwood J A, Hirji N, Zaman S, Jones P R, Schwarzkopf D S, Rees G, *et al.* (2022) A demonstration of cone function plasticity after gene therapy in achromatopsia. *Brain* **145**:3803-3815 https://doi.org/10.1093/brain/awac226 | PubMed

21. **Henriksson L,** Nurminen L, Hyvarinen A, Vanni S (2008) Spatial frequency tuning in human retinotopic visual areas. *Journal of Vision* **8**:5-5 https://doi.org/10.1167/8.10.5 | PubMed

22. **Hertle R W,** Yang D, Cochran M, Edward P R (2017) Clinical Contrast Sensitivity Function in Patients with Infantile Nystagmus Syndrome Before and After Eye Muscle Surgery. *Journal of Ophthalmology & Clinical Research* **4**:1-8 https://doi.org/10.24966/OCR-8887/100033

23. **Himmelberg M M,** Winawer J, Carrasco M (2020) Stimulus-dependent contrast sensitivity asymmetries around the visual field. *Journal of Vision* **20**:1-19 https://doi.org/10.1167/jov.20.9.18 | PubMed

24. **Himmelberg M M,** Winawer J, Carrasco M (2023) Polar angle asymmetries in visual perception and neural architecture. *Trends in Neurosciences* **46**:445-458 https://doi.org/10.1016/j.tins.2023.03.006 | PubMed

25. **Horton J C,** Hoyt W F (1991) The Representation of the Visual Field in Human Striate Cortex: A Revision of the Classic Holmes Map. *Archives of Ophthalmology* **109**:816-824 https://doi.org/10.1001/archopht.1991.01080060080030 | PubMed

26. **Kurzawski J W,** Gulban O F, Jamison K, Winawer J, Kay K (2022) Non-Neural Factors Influencing BOLD Response Magnitudes within Individual Subjects. *Journal of Neuroscience* **42**:7256-7266 https://doi.org/10.1523/JNEUROSCI.2532-21.2022 | PubMed

27. **Lange R,** Kumagai A, Weiss S, Zaffke K B, Day S, Wicker D, Howson A, Jayasundera K T, Smolinski L, Hedlich C, *et al.* (2021) Vision-related quality of life in adults with severe peripheral vision loss: A qualitative interview study. *Journal of Patient-Reported Outcomes* **5**:7 https://doi.org/10.1186/s41687-020-00281-y | PubMed

28. **Lisboa R,** Chun Y S, Zangwill L M, Weinreb R N, Rosen P N, Liebmann J M, Girkin C A, Medeiros F A (2013) Association between rates of binocular visual field loss and vision-related quality of life in patients with glaucoma. *JAMA Ophthalmology* **131**:486-494 https://doi.org/10.1001/jamaophthalmol.2013.2602 | PubMed

29. **Liu T,** Heeger D J, Carrasco M (2006) Neural correlates of the visual vertical meridian asymmetry. *Journal of Vision* **6**:12-12 https://doi.org/10.1167/6.11.12 | PubMed

30. **O'Connell C,** Ho L C, Murphy M C, Conner I P, Wollstein G, Cham R, Chan K C (2016) Structural and functional correlates of visual field asymmetry in the human brain by diffusion kurtosis MRI and functional MRI. *NeuroReport* **27**:1225-1231 https://doi.org/10.1097/WNR.0000000000000682 | PubMed

31. **Oliva A** (2005) CHAPTER 41—Gist of the Scene. In: Itti L, Rees G, Tsotsos J K (Eds). *Neurobiology of Attention* Academic Press. pp. 251-256 https://doi.org/10.1016/B978-012375731-9/50045-8

32. **Pawloff M,** Linhardt D, Woletz M, Hummer A, Sacu S, Vasileiadi M, Garikoitz L U, Holder G, Schmidt-Erfurth U M, Windischberger C, *et al.* (2023) Comparison of Stimulus Types for Retinotopic Cortical Mapping of Macular Disease. *Translational Vision Science and Technology* **12**:1-13 https://doi.org/10.1167/tvst.12.3.6 | PubMed

33. **Prabhakaran G T,** Al-Nosairy K O, Tempelmann C, Thieme H, Hoffmann M B (2021) Mapping Visual Field Defects With fMRI – Impact of Approach and Experimental Conditions. *Frontiers in Neuroscience* **15**:745886 https://doi.org/10.3389/fnins.2021.745886 | PubMed

34. **R Core Team** (2023) *R: A Language and Environment for Statistical Computing* R Foundation for Statistical Computing. https://www.R-project.org/

35. **Rai B,** Sabeti F, Carle C, Maddess T (2024) Visual Field Tests: A Narrative Review of Different Perimetric Methods. *Journal of Clinical Medicine* **13**:2458 https://doi.org/10.3390/jcm13092458 | PubMed

36. **Randall D,** Fox S L, Fenner J W, Arblaster G E, Bjerre A, Griffiths H J (2020) Using VR to Investigate the Relationship between Visual Acuity and Severity of Simulated Oscillopsia. *Current Eye Research* **45**:1611-1618 https://doi.org/10.1080/02713683.2020.1772834 | PubMed

37. **Ribeiro F L,** Bollmann S, Puckett A M (2021) Predicting the retinotopic organization of human visual cortex from anatomy using geometric deep learning. *NeuroImage* **244**:118624 https://doi.org/10.1016/j.neuroimage.2021.118624 | PubMed

38. **Ritter M,** Hummer A, Ledolter A A, Holder G E, Windischberger C, Schmidt-Erfurth U M (2019) Correspondence between retinotopic cortical mapping and conventional functional and morphological assessment of retinal disease. *British Journal of Ophthalmology* **103**:208-215 https://doi.org/10.1136/bjophthalmol-2017-311443 | PubMed

39. **Roelofzen C,** Daghlian M, van Dijk J A, de Jong M C, Dumoulin S O (2025) Modeling neural contrast sensitivity functions in human visual cortex. *Imaging Neuroscience* **3**:imag_a_00469 https://doi.org/10.1162/imag_a_00469 | PubMed

40. **Roh M,** Selivanova A, Shin H J, Miller J W, Jackson ML (2018) Visual acuity and contrast sensitivity are two important factors affecting vision-related quality of life in advanced age-related macular degeneration. *PLoS ONE* **13**:1-12 https://doi.org/10.1371/journal.pone.0196481 | PubMed

41. **Ross J,** Morrone M C, Goldberg M E, Burr D C (2001) Changes in visual perception at the time of saccades. *Trends in Neurosciences* **24**:113-121 https://doi.org/10.1016/S0166-2236(00)01685-4 | PubMed

42. **Rovamo J,** Leinonen L, Laurinen P, Virsu V (1984) Temporal Integration and Contrast Sensitivity in Foveal and Peripheral Vision. *Perception* **13**:665-674 https://doi.org/10.1068/p130665 | PubMed

43. **Rovamo J,** Virsu V (1979) An estimation and application of the human cortical magnification factor. *Experimental Brain Research* **37**:495-510 https://doi.org/10.1007/BF00236819 | PubMed

44. **Sereno M I,** Dale A M, Reppas J B, Kwong K K, Belliveau J W, Brady T J, Rosen B R, Tootell R B H (1995) Borders of Multiple Visual Areas in Humans Revealed by Functional Magnetic Resonance Imaging. *Science* **268**:889-893 https://doi.org/10.1126/science.7754376 | PubMed

45. **Subhi H,** Latham K, Myint J, Crossland M D (2017) Functional visual fields: Relationship of visual field areas to self-reported function. *Ophthalmic and Physiological Optics* **37**:399-408 https://doi.org/10.1111/opo.12362 | PubMed

46. **Tailor V K,** Theodorou M, Dahlmann-Noor A H, Dekker T M, Greenwood J A (2021) Eye movements elevate crowding in idiopathic infantile nystagmus syndrome. *Journal of Vision* **21**:9 https://doi.org/10.1167/jov.21.13.9 | PubMed

47. **Welbourne L E,** Morland A B, Wade A R (2018) Population receptive field (pRF) measurements of chromatic responses in human visual cortex using fMRI. *NeuroImage* **167**:84-94 https://doi.org/10.1016/j.neuroimage.2017.11.022 | PubMed

48. **World Health Organization** (2019) WHO launches first World report on vision. https://www.who.int/news/item/08-10-2019-who-launches-first-world-report-on-vision

49. **Xu J,** Moeller S, Auerbach E J, Strupp J, Smith S M, Feinberg D A, Yacoub E, Uğurbil K (2013) Evaluation of slice accelerations using multiband echo planar imaging at 3T. *NeuroImage* **83**:991-1001 https://doi.org/10.1016/j.neuroimage.2013.07.055 | PubMed

Chow-Wing-Bom H, Lisi M, Benson N, Lygo-Frett F, Yu-Wai-Man P, Dick F, Maison-Mor R, Dekker T (2026) Dataset for Chow-Wing-Bom et al., 2025, eLife. Zenodo. https://doi.org/10.5281/zenodo.19051438

Peer reviews

Reviewer #1 (Public review):

Integrating large-field stimulation with a retinotopic atlas, this study introduces an fMRI-based method for measuring contrast sensitivity across the visual field. Retinotopy was assessed using pRF mapping and a calibrated Benson atlas. The authors validate their method by replicating known patterns of contrast sensitivity across eccentricities and visual field quadrants in healthy subjects, and demonstrate its potential clinical utility through case studies of both simulated and real visual field loss.

Comments on revisions:

I appreciate the addition of the quadrant-scotoma condition and the authors' clarification that the goal is to demonstrate individual-level detection sensitivity. The 95% CI argument is reasonable, and I am satisfied with framing the simulated-scotoma work as proof-of-concept.

https://doi.org/10.7554/eLife.105930.2.sa3

Reviewer #2 (Public review):

Summary

This study uses functional MRI to evaluate visual contrast sensitivity across the visual field at the level of the visual cortex, testing the method as a proof of principle in a small group of normally sighted individuals, modelling both normal vision and simulated vision loss, as well as a patient with independently verified vision loss. The results suggest a promising technique to measure vision objectively across the visual field and overcomes the requirement for careful fixation which is often challenging in those with low vision or sight loss.

Strengths

• Objective measure of central vision: The proposed method may provide a more comprehensive and objective assessment of residual visual function in individuals with sight loss. This may be particularly useful for those with central visual field loss without the requirement of stable fixation or subjective motor responses.

• More sensitive measure: The use of slope to calculate contrast sensitivity across a range of contrasts within the brain is clever and likely more sensitive than single threshold measurements or standard clinical measures of visual acuity using letter charts. Standard supra-threshold (high contrast) tests are not ideal for capturing residual vision or partial vision loss.

• Good agreement with standard atlas: The Benson atlas provides a good estimate of visual field maps within V1 based on anatomical landmarks, and the authors take steps to refine this informed by cortical magnification and V1 surface area (brain size) for each individual participant. This could allow the technique to be generalised without the need to collect lengthy individual mapping data from every participant.

• Within-subject reproducibility: The measurements appear to be sensitive and reproducible, particularly in those with normal vision, and are consistent with known features of visual sensitivity differences in different parts of the visual field.

• Potential tool to measure visual field sensitivity in controls: Even if the proposed methods are not ideal for widespread clinical translation, they do offer an exciting tool to test hypotheses about visual field differences in healthy controls. For example, there seems to be an increase in sensitivity on either side of the simulated ring scotoma (Fig 6 - perhaps due to the release of lateral inhibition?). Reliability measures suggest that individual differences are consistent in healthy controls (although not tested statistically, perhaps due to the small sample size?). Whether they reflect behaviourally meaningful differences in visual field sensitivity could be tested in individuals by comparing them to behavioural measures across the visual field.

• Potential tool to test novel treatments: The proposed techniques could be used to test within-subject changes in visual function in environments that are equipped to measure and analyse fMRI data, including clinical trials aimed at determining the success of novel treatments. Preliminary testing in healthy controls with eye movements also suggests that the method is suitable for testing low vision patients with unstable fixation (e.g., nystagmus), and the authors have modelled the effects of varying amounts and types of eye movements on functional outcome measures.

Weaknesses

• Questionable sensitivity to differences in patients. The variability in heat maps across healthy control participants is somewhat surprising, and it is uncertain whether they represent actual visual sensitivity differences or an artifact of the measurement technique, e.g., due to signal-to-noise differences introduced by local variations in brain anatomy. Thus, it is uncertain whether the substantial variance across controls will allow for a sufficiently stable baseline to detect meaningful differences in individual patients. Also, as the authors rightly point out, Benson atlas does not model differences along meridians, so that upper/lower field differences might not be detectable. However, the authors acknowledge that this is a pilot study, and further testing a wider range of scotoma types in patients and simulated in controls will only improve the methods. Furthermore, the ability to capture visual field representations in human visual cortex is also likely to improve with computational advances, making the use of atlases more feasible, obviating the need for individualised population receptive field mapping.

• Potential for clinical translation. Although it is a sensitive measure, functional MRI is costly, is not available in all clinical settings, requires significant post-processing analyses, and may be contraindicated in some individuals due to safety (e.g., metallic implants) or other concerns (e.g., claustrophobia). These could present significant barriers to widespread clinical translation, if this were the ultimate goal of the study.

• Limited range of spatial frequencies. The spatial frequencies tested were still quite low (0.3 and 3cpd) compared to measures such a visual acuity. Extending the measurements to higher spatial frequencies could allow better characterization of central vision, although necessarily for peripheral vision. However, this may depend on the typical visual abilities of the patient population of interest.

Appraisal and Impact:

The authors used appropriate and robust methods to assess and model known features of visual sensitivity differences across the visual field in sighted controls. In addition, the assessment technique successfully captured sensitivity changes due to simulated and actual partial field loss but was also fairly resilient to eye movements and fixation instability, typical of patients with sight loss. Although currently providing a proof of principle, the method is likely to improve with further testing and increasing normative sample sizes, and as computational methods continue to advance visual field map predictions. Although it may not be adopted widely as a standard clinical assessment technique due to the expense and other obstacles, it would provide a valuable tool in assessing clinical populations, for example in the context of clinical trials to assess suitability for treatment interventions or monitor treatment outcomes.

https://doi.org/10.7554/eLife.105930.2.sa2

Reviewer #3 (Public review):

Summary:

Chow-Wing-Bom et al. introduce an innovative wide-field visual stimulation setup for 3T experiments that enables stimulation up to a diameter of 40{degree sign} visual angle while allowing continuous gaze tracking. Using this setup, the authors systematically investigate contrast sensitivity across the visual field by presenting subjects with sinusoidal gratings varying in contrast and spatial frequency. Their findings confirm the expected organization of contrast sensitivity, demonstrating a preference for high spatial frequencies in the central field and lower frequencies in the periphery. They also extend these measurements to eccentricities up to 20{degree sign}, which exceeds previous fMRI-based reports. Moreover, the study explores the potential of using contrast sensitivity calculations as a method for detecting visual field defects, demonstrated in a healthy subject with simulated ring-shaped and upper-right-quadrant scotomas, and in a patient with LHON. The revised version additionally characterises the robustness of the approach to varying degrees of fixation instability.

Strengths:

- The manuscript is well written and provides comprehensive methodological details, ensuring high transparency and reproducibility.

- The visual stimulation setup represents a significant technical advance by enabling wide-field stimulation with continuous eye tracking, which is crucial for both research and potential clinical applications.

- The study confirms established findings regarding the organization of contrast sensitivity while extending them to a larger eccentricity range.

- The efforts to establish a measure for visual field losses aligns with current efforts to develop objective alternatives to conventional perimetry.

- The revised manuscript includes an empirical assessment of how varying levels of eye movement affect cortical contrast sensitivity estimates, providing useful guidance on the

tolerance of the approach to fixation instability.

Weaknesses:

- The original version left certain methodological aspects unclear, particularly the correction of eccentricity values from the Benson atlas and the V1 masks used in each analysis branch. The authors have added a dedicated figure illustrating the eccentricity correction procedure and now explicitly state that a manually delineated V1 mask was used for the pRF-based analyses while the Benson V1 label was used for the atlas-based analyses, together with a discussion of how this difference may influence the comparison.

- Minor inconsistencies in reporting, such as the introduction of a second session in the Results section, have been corrected.

The conclusion that high-contrast patterns as in pRF mapping are not optimal to test for subtle but potentially clinically relevant changes in the visual field coverage are very valid. The suggested use of contrast sensitivity can therefore be a potentially well-suited parameter for estimating visual field losses. The presented work is an interesting starting point, and the proposed method of using contrast sensitivity as measure for partial vision loss should be further explored.

Comments on revisions:

The authors have thoroughly addressed all points raised in my original review, and I have no further concerns.

https://doi.org/10.7554/eLife.105930.2.sa1

Author response:

The following is the authors' response to the original reviews

> ***Reviewer #1 (Public review):***
>
> *The current claims should be better supported by more evidence.*
>
> *R1-1: In the first experiment, have the statistics undergone multiple comparison corrections (e.g., Line 441-442)? Given the small sample size, incorporating additional statistical tests (such as the Bayes Factor) could strengthen the analysis.*

We confirm that corrections for multiple comparisons are now applied where appropriate, particularly in the group-level ANOVA analyses.

"Post-hoc tests using Holm-Bonferroni correction show that V1 neuronal populations receiving inputs from the central visual field (0.5-4.5°) showed greater contrast sensitivity to high spatial frequency as compared to low spatial frequency stimuli (steeper slope for the 3cpd versus 0.3cpd condition: 0.5-2.5°: $t(6) = 4.35$, $p_{bonf} = 0.0149$; 2.5-4.5°: $t(6) = 3.471$, $p_{bonf} = 0.0266$). Conversely, peripheral eccentricities in V1 (above 9.5°) showed higher contrast sensitivity to low as compared to high spatial frequency stimuli (steeper slope for 0.3cpd versus 3cpd condition: 9.5-15°: $t(6) = -4.591$, $p_{bonf} = 0.0149$; 15-20°: $t(6) = -6.615$, $p_{bonf} = 0.0029$). Between 4.5° and 9.5°, V1 contrast sensitivity was similar for both spatial frequencies ($t(6) = -0.226$, $p_{bonf} = 0.8286$). Crucially, these effects remained when using retinotopic estimates based on structural scans derived from the Benson retinotopic atlas instead of the pRF-mapping measures (0.5-2.5°: $t(6) = 5.768$, $p_{bonf} = 0.0059$; 2.5-4.5°: $t(6) = 2.531$, $p_{bonf} = 0.0892$; 4.5-9.5°: $t(6) = -0.293$, $p_{bonf} = 0.7792$; 9.5-15°: $t(6) = -3.274$, $p_{bonf} = 0.0509$; 15-20°: $t(6) = -3.528$, $p_{bonf} = 0.0496$; see Figure A2 and Table A3 in Appendix section)."

"Post-hoc pairwise comparisons using Holm-Bonferroni corrections revealed that, as predicted, the cortical contrast response function had a higher slope – indicating better V1 sensitivity – along the horizontal versus vertical quadrants (Horizontal-Vertical Anisotropy – HVA: $t(6) = 5.908$, $p_{bonf} = 0.0031$) and along the lower versus upper quadrant (Vertical Meridian Anisotropy – VMA: $t(6) = 4.106$, $p_{bonf} = 0.0126$). Conversely, no difference in cortical contrast sensitivity was found between V1 neuronal populations encoding the left and right quadrants of the visual field (Left-Right Horizontal Meridian Anisotropy – LRHMA: $t(6) = 0.7197$, $p_{bonf} = 0.4988$)."

"We found that the horizontal-vertical anisotropy effect was recovered (HVA: $t(6) = 3.584$, $p_{bonf} = 0.0347$), but that the vertical meridian anisotropy effect was not (VMA: $t(6) = 0.744$, $p_{bonf} = 0.9697$) with this approach."

> *R1-2a: The authors claim that "structure-based atlases can replace the need for pRF mapping in cases where it might otherwise be difficult or impossible to collect pRF data." This claim needs further scrutiny. Currently, only one simulated condition of visual field loss was examined in one subject.*

AR-R1-2a: We agree that further work is needed to fully establish the utility of structure-based atlases. As a first step, we have followed the reviewer's suggestion and collected an additional dataset from one of the seven participants, in whom we simulated another condition of visual field loss – specifically, loss of the upper right quadrant. This participant is the same individual already presented in the manuscript (C5), but with a different simulated vision loss condition.

This new condition has been introduced in the Methods, Results and Discussion section, and a new Figure 10 alongside Figure 9 which showed the 3º-8º scotoma. With relevant changes as follows:

"We also demonstrate the clinical relevance of this approach by recovering simulated scotomas (i.e., a ring of visual field loss around fixation and the loss of an entire visual field quadrant), as well as visual field loss in a patient with a neurodegenerative disorder causing large areas of visual field loss."

"Additionally, one participant (C5) repeated the task under two simulated vision loss conditions (ring or quadrant loss), and two others (C5, C6) completed it with different levels of eye movement."

"Simulated vision loss

One healthy control participant (C5) also performed a version of the task designed to simulate two forms of visual input loss (i.e., artificial scotoma). These simulations were implemented by: (a) masking a region of the visual field with a grey, annular ring, covering 3º-8º eccentricity, and (b) masking the upper right visual quadrant using a grey quarter-sector overlay. The stimuli and contrast levels used in this task were identical to those described in the original task."

"A test-case of simulated loss of visual inputs

In the previous sections, we showed that the slope of a square root function provides a reliable measure of contrast sensitivity in the brain of healthy controls. But can this brain-level model also quantify loss of visual inputs? To test this, we first simulated an artificial scotoma in one normal sighted participant, by (a) masking a region of the visual field with a grey, annular ring, covering 3°-8° eccentricity (Figure 9A), and (b) masking the upper-right visual quadrant using a grey quarter-sector overlay (Figure 10A). We expect smaller slope

values in V1 neuronal populations that would under normal circumstances encode that part of the visual space.

As expected, we observed reduced responses in V1 locations corresponding to the artificial scotoma (Figures 9 and 10), with increased responses along the edges of the mask for the ring scotoma condition (Figure 9B). This artificial loss of visual input was also clearly present in the cortical contrast sensitivity estimate, with significantly reduced slope steepness in V1 between 3-8° for the ring scotoma condition (Figure 9C&D) and in the upper-right quadrant for the quarter-sector scotoma condition (Figure 10B&C). Additionally, we could recover this scotoma using the calibrated Benson template, although less accurately (Figures 9E and 10D). These results show that this measure of V1 contrast sensitivity is sensitive enough to detect loss of visual inputs in the brain at an individual level, when a complete local loss of sight is simulated, and that this approach does not crucially rely on pRF mapping data from the individual. This supports the utility of our approach in recovering patterns of vision loss and recovery at a cortical level."

"Mapping Simulated and Pathology-Driven Vision Loss

Our method successfully identified both simulated retinal loss in a healthy volunteer and real visual field loss in a patient with Leber Hereditary Optic Neuropathy (LHON). The signal drop observed in response to masking portions of the visual field in the healthy control was both large and significant at the individual level, as demonstrated by non-overlapping 95% confidence intervals (Figures 9B-C and 10B). This provides proof-of-concept evidence that our approach can detect signal changes in individual patients, which is a critical requirement for clinical translation.

Unlike previous fMRI studies that used high-contrast stimuli (Farahbakhsh et al., 2022; Pawloff et al., 2023; Ritter et al., 2019), which may not accurately represent partial vision loss due to potential saturation effects and the stimulation of less sensitive retinal cells, our use of multiple contrast levels offers a more nuanced assessment of cortical contrast sensitivity.

Combined with the large-field set-up allowing stimulation up to 20° eccentricity, this approach may be particularly well-suited for evaluating treatment efficacy in cases of widespread and variable vision loss.

Future work will focus on further validating reconstruction accuracy under controlled conditions, including simulated scotomas of varying severity and location, expanding testing to larger patient cohorts, and establishing a normative dataset to contextualize patient data.

> *R1-2b: Also, in Figure 7, contrast sensitivity in the periphery differs between pRF mapping and the Benson atlas. How do the authors explain this discrepancy?*

AR-R1-2b: The discrepancy in periphery between pRF mapping and Benson atlas is caused by various factors. These include (a) individual differences in the retinotopy/structure relationship that are not captured in the template, (b) the fact that the Benson atlas at larger eccentricities was obtained with hemifield stimulation, and (c) a larger impact of any inaccuracies at larger eccentricities because of cortical magnification. As a result, peripheral vertices are more likely to be mis-assigned by the template than central ones. Note that this adds distortion in cortical visual field maps which will be consistent across timepoints (rather than noise). Critically, a reduction in accuracy does not preclude utility if meaningful differences in spatial patterns in cortical sensitivity can still be recovered, as is the case in our data. We cover this in the discussion.

"Particularly at large eccentricities however, we initially observed inaccuracies between the template and individual retinotopy eccentricity estimates which led to substantial distortions in cortical visual field maps due to cortical magnification (see Figure A4 in Appendix section).

To address this, we adjusted the Benson eccentricity estimates to align with the cortical magnification scaling function (Horton & Hoyt, 1991)."

"Beyond ROI considerations, we still observed differences in cortical sensitivity between pRF mapping and the adjusted Benson atlas - particularly in the periphery. Several factors likely contribute to this. First, individual differences in the relationship between cortical structure and retinotopy are not fully captured by the template. Second, the Benson atlas has never been fit with empirical data more eccentric than approximately 20°, which naturally limits its precision in the far periphery. Third, because of cortical magnification, any small inaccuracy at larger eccentricities has a disproportionately large effect, making peripheral vertices more susceptible to mis-assignment than central ones. These influences introduce systematic distortions in cortical visual field maps rather than random noise and thus remain consistent across time points - an important point when assessing longitudinal changes (e.g., ageing or gene-therapy interventions). Importantly, the spatial gradients in cortical contrast sensitivity were preserved across both the pRF and Benson atlas approaches, indicating that minor ROI differences do not affect our conclusions. Together, these findings show that the Benson Atlas remains a useful alternative when pRF mapping is not feasible.

> *R1-3: Overall, the writing could be significantly improved.*

AR-R1-3: We have made edits throughout the manuscript and hope this has improved the writing.

> ***Reviewer #1 (Recommendations for the authors):***
>
> *R1-Recommendation 1a: The writing can be significantly improved for clarity.*
>
> *The introduction section is not well-organized, and the motivation for developing the current method (Paragraphs 2-3) is vague and lacks adequate documentation.*
>
> *Several references are missing (e.g., Lines 90-92) or incorrectly placed (e.g., Lines 108-109).*

AR-R1-Recommendation 1a: We have revised the Introduction to clarify the motivation for developing the current method and to correct missing or misplaced references.

"Still, testing visual function across the visual field remains limited in clinical and therapeutic contexts, especially in patients with drastic central vision loss. In this study, we aimed to address this gap by introducing a novel fMRI-based approach to measure visual field sensitivity across a wide expanse of the visual field (40º diameter)."

"Beyond visual acuity, functional impairment across the wider visual field can be measured using a range of visual field tests, from the finger counting visual confrontation field test to more complicated and/or computerized tests (e.g., standard automatic perimetry, kinetic perimetry, microperimetry; Rai et al., 2024). Computerized tests typically involve measuring sensitivity to the luminance contrast of a target relative to a background at different visual field locations while the participant's gaze is fixed on a central point. In some cases (e.g., microperimetry), sensitivity measurements are paired with fundus imaging, offering greater precision in linking visual field functions to specific retinal locations (Rai et al., 2024). As a result, visual field assessments can reveal functionally relevant deficits – including localized sensitivity loss and scotomas – that are not captured by foveal acuity alone, and are therefore potentially valuable for tracking disease progression and therapeutic efficacy.

Despite their clinical relevance, visual field testing comes with challenges and limitations, and as a result, the inclusion of visual field measures in sight-rescuing therapy trials is limited. Firstly, it requires prolonged fixation and sustained visual attention. This can be very challenging for patients with severe vision loss, who often struggle to fixate, and strain to

detect even high intensity stimuli. This can lead to long and unpleasant testing sessions with unreliable results. Secondly, as perception of light stimuli is inherently subjective (Rai et al., 2024) and effortful, patients may vary in their criteria for visual recognition, and in their ability to report visual signals that are weakened or distorted by disease. Together, these constraints reduce the feasibility, robustness, and interpretability of conventional visual field testing in clinical trials, underscoring the need for alternative or complementary approaches that can assess functional vision while placing fewer demands on subjective reporting."

"Functional MRI (fMRI) has recently been proposed as a promising alternative to measure visual field loss, as it requires no overt task, and instead measures visual sensitivity directly from brain responses (Farahbakhsh et al., 2022; Prabhakaran et al., 2021; Ritter et al., 2019). Population receptive field (pRF) mapping fMRI can measure which parts of the cortex respond to which parts of the visual scene (Dumoulin & Wandell, 2008)."

"Finally, most studies use a single maximum contrast stimulus to assess visual function (Broderick et al., 2022; Farahbakhsh et al., 2022; Liu et al., 2006; O'Connell et al., 2016; Ritter et al., 2019)."

> *R1-Recommendation 1b: The strengths of the current method and its applicable scenarios are unclear. For example, in Lines 39-40: "We developed an fMRIbased approach to measure contrast sensitivity across the visual field without the need for precise fixation." To what extent can fixation be imprecise? Could this protocol be applied to patients with strabismus, who have biased fixation?*

AR-R1-Recommendation 1b: We agree with the reviewer that the tolerance to fixation challenges is key here and so we collected additional data to respond to your points regarding the effects of eye movement on the cortical contrast sensitivity maps.

In terms of biased fixation, the approach should be very robust to this, as this would just reduce the cortical visual field covered on one side and extend it on the other.

We collected new data to test the tolerance to fixation instability across a wide range of eye movement, including severe nystagmus-level movement. Despite large eye movements, the cortical contrast-sensitivity pattern remained largely consistent, though extreme movements reduced slope estimates and flattened the cortical sensitivity pattern for 3cpd, indicating reduced measurement sensitivity for extreme eye movement to high spatial frequency gratings.

These additions have been incorporated into the Abstract, Methods, Results, and Discussion sections as follows:

Abstract

"To assess the method's tolerance to fixation variability, we further investigated how different levels of eye movement affect cortical sensitivity patterns in two participants. We found that cortical sensitivity patterns were largely preserved across eye movement, particularly at low spatial frequencies. This suggests that our approach can accommodate several degrees of fixation instability, making it suitable for populations with unstable or biased fixation for whom visual field maps are harder to acquire behaviorally (e.g., patients with dense central scotoma or strabismus)."

Methods

"Additionally, one participant (C5) repeated the task under two simulated vision loss conditions (ring or quadrant loss), and two others (C5, C6) completed it with different levels of eye movement."

Results

“Effect of eye movement

Participants C5 and C6 also performed a version of the task designed to test the effect of eye movements. In this version, saccades were elicited by randomly and rapidly shifting the fixation dot away from central fixation (C5: 2º and 5º from fixation and random motion; C6: up to 2º from fixation). Participant C5 was tested using 0.3 and 3cpd gratings at four contrast levels (7.5, 42.2, 60, 100%), while participant C6 was tested only under the low spatial frequency condition (0.3cpd).

Fixation stability was assessed for each fMRI run using the bivariate contour ellipse area (BCEA), which estimates the area (in degrees^2 or arcmin^2) of an ellipse that contains approximately 95% of fixation points. BCEA was calculated using the formula: , as described by Morales et al. (2016). In this expression, σ_h and σ_v represent the standard deviations of eye position in the horizontal and vertical directions, respectively, while p corresponds to the Pearson correlation coefficient between horizontal and vertical eye positions. The constant k determines the size of the ellipse based on the desired probability area, defined by the relationship $P = 1 - e^{-k}$, with P set to 0.95 in this study. A smaller BCEA indicates greater fixation stability.

“Effect of eye movements on V1 cortical sensitivity

So far, we have demonstrated that our measure of cortical sensitivity can reliably recover known gradients in sensitivity across eccentricities and visual quadrants. We also showed that this measure was consistent across visits and sessions, suggesting its potential utility for monitoring changes over time. However, all prior tasks were conducted under conditions of central fixation, with participants instructed to maintain gaze on a central dot. A key motivation for this approach was its theoretical robustness to fixation instability. We therefore also aimed to investigate how varying degrees of eye movement might influence cortical sensitivity across the visual field.

To address this, two participants (C5 and C6) completed a modified version of the contrast sensitivity task in which they made eye movements either by following a dot moving randomly at a radius of 2º or 5º around fixation, or by self-initiated very large eye movements. Eye movements across these or by self-initiated very large eye movements. Eye movements across these conditions (Figure 7, bottom row; Figure 8, bottom row), were quantified using BCEA (C5 – Central fixation: mean±SD = 0.57±0.11 deg^2, 2º eye motion: 2.69±0.48 deg^2, 5º eye motion: 20.3±1.32 deg^2, random eye motion: 133.7±23.36 deg^2; C6 – Central fixation: 0.96±0.56 deg^2, 2º eye motion: 1.28±0.15 deg^2). For reference, in severe (idiopathic) nystagmus, the eye movement variability along the vertical and horizontal planes is on average 1.08 deg and 1.60 deg, respectively (Tailor et al., 2021). Assuming a moderate correlation between axes (p = 0.3), the average fixation stability would equate to a BCEA of ~21.46 deg^2 (i.e., ~5º eye motion condition in our data).

Despite these very large levels of eye movements, we observed that the overall cortical contrast sensitivity spatial pattern across eccentricity remained remarkably consistent (Figure 7, top and middle rows; Figure 8, top row). However, at the most extreme movements, contrast sensitivity estimates (slope values) were lower; and while the overall cortical visual field map structure was still clearly present for low spatial frequencies, it appeared more flattened for 3cpd, suggesting reduced sensitivity of our measure for large eye movement and high spatial frequency stimuli.”

Discussion

"Crucially, one advantage of cortical visual field mapping is that the maps are inherently centered on the foveal confluence, providing a stable reference point for comparing responses across eccentricities. When combined with large-field, spatially homogeneous stimuli, this anchoring means that our approach should remain robust to moderate fixation variability and still quantify sensitivity changes across the visual field – provided that fixation instability does not exceed the stimulus extent (40º diameter).

When measuring the impact of eye movements, we found that spatial sensitivity patterns were largely preserved, even for extreme eye movements (emulating severe nystagmus). However, under the most extreme conditions, sensitivity estimates (i.e., slope values) were reduced, especially for high spatial frequency (SF) stimuli. This likely reflects image blurring from large rapid eye movements, which degrades high-SF inputs and shifts activation toward neurons tuned to lower SFs. This aligns with evidence that nystagmus and large saccades impair perception of fine detail and grating stimuli due to retinal image slip (Abadi & Bjerre, 2002; Dickinson & Abadi, 1985; Hertle et al., 2017; Randall et al., 2020). While classic findings report suppression of low-SF signals during saccades (Burr et al., 1994; Ross et al., 2001), our results suggest that high SF sensitivity may be more vulnerable to large eye movements when participants are presented with 2Hz phase-flickering gratings. Further validation in clinical groups with naturally-occurring fixation instability would further strengthen these conclusions."

> *R1-Recommendation 1c: There are also some confusing descriptions, such as Lines 130-132.*

AR-R1-Recommendation 1c: We have also clarified ambiguous descriptions of the Benson atlas templates.

"We therefore also evaluated the approach using the structure-based atlas of retinotopic values developed by Benson et al. (Benson et al., 2014; Benson & Winawer, 2018). This atlas predicts retinotopic organization by aligning individual cortical anatomy (e.g., surface curvature) to a group-average template that incorporates an algebraic model of retinotopy (Benson et al., 2014). Once the subject's brain is aligned to this structural atlas, retinotopic maps defined by the model – i.e., polar angle and eccentricity maps – are projected onto the individual's cortex. This allows estimation of visual field maps without requiring functional imaging, and provides a non-invasive, anatomy-driven approximation of visual field representations."

> *R1-Recommendation 1d: Line 361: "Assessing the brain's ability to discriminate shapes"-is the author referring to the functional relevance of contrast tuning assessment here? Since the task or stimuli are not related to shapes, this description is unclear.*

AR-R1-Recommendation 1d: We have revised the reference to "discriminating shapes" to more accurately reflect the functional relevance of contrast sensitivity mapping.

"To measure visual field function, we developed a new measure of cortical contrast sensitivity, assessing the brain's ability to discriminate gratings of varying spatial frequencies based on luminance variations."

> *R1-Recommendation 2a: Simulated visual loss experiment: only one condition of visual field loss was examined in a single subject. I encourage the authors to include additional subjects to meet statistical test criteria at group level. Simulated scotomas in more visual quadrants, including both central and peripheral areas, should be examined, as asymmetries may exist.*

AR-R1-Recommendation 2a: We agree that it is important to verify that the approach can also capture other types of scotomas. We have therefore now incorporated another simulated

condition of visual field loss, namely loss of the upper right quadrant.

Regarding adding more participants: The drop in signal is clearly large and significant at the individual level (error bars corresponding to 95% confidence interval do not overlap; Figures 9B-C & 10B). The ability to detect signal change at the individual level is what we need for clinical application, and here we are showing proof-of-concept of its feasibility with our approach. However, we do appreciate that it might be valuable to test cortical visual field loss reconstruction accuracy with simulated scotomas of varying levels of vision loss in variable locations. We now highlight this as a future direction.

Please refer to our response to R1-2a, where we also detail the corresponding changes made in the manuscript.

> *R1-Recommendation 2b: Additionally, why do the results from pRF mapping and the corrected Benson atlas differ, particularly in the far periphery?*

AR-R1-Recommendation 2b: Please refer to our response to R1-2b, where we also detail the corresponding changes made in the manuscript.

> *R1-Recommendation 3: To validate the recovery of visual field loss in the case study, it would be necessary to include fundus imaging to characterize the structural loss and correlate it with the behavioral and fMRI results.*

AR-R1-Recommendation 3: We included Compass perimetry data for the LHON patient, which is fundus-tracked perimetry and uses fundus imaging to keep the visual stimulation fixed to retinal locations.

In the context of LHON, the fundus image is not expected to provide more information than perimetry. This is because the visual deficit in LHON arises from optic nerve dysfunction, and retinal abnormalities are typically minimal. Aside from the characteristic pallor of the optic disc, the fundus appearance is usually normal in appearance.

For illustration, Author response image 1 shows the Compass-acquired fundus image from the LHON patient included in this study. For comparison, we also show a normal fundus image from a 25-year-old male volunteer, reproduced from Häggström, Mikael (2014). "Medical gallery of Mikael Häggström 2014". WikiJournal of Medicine 1 (2). DOI:10.15347/wjm/2014.008. ISSN 2002-4436. Public Domain.

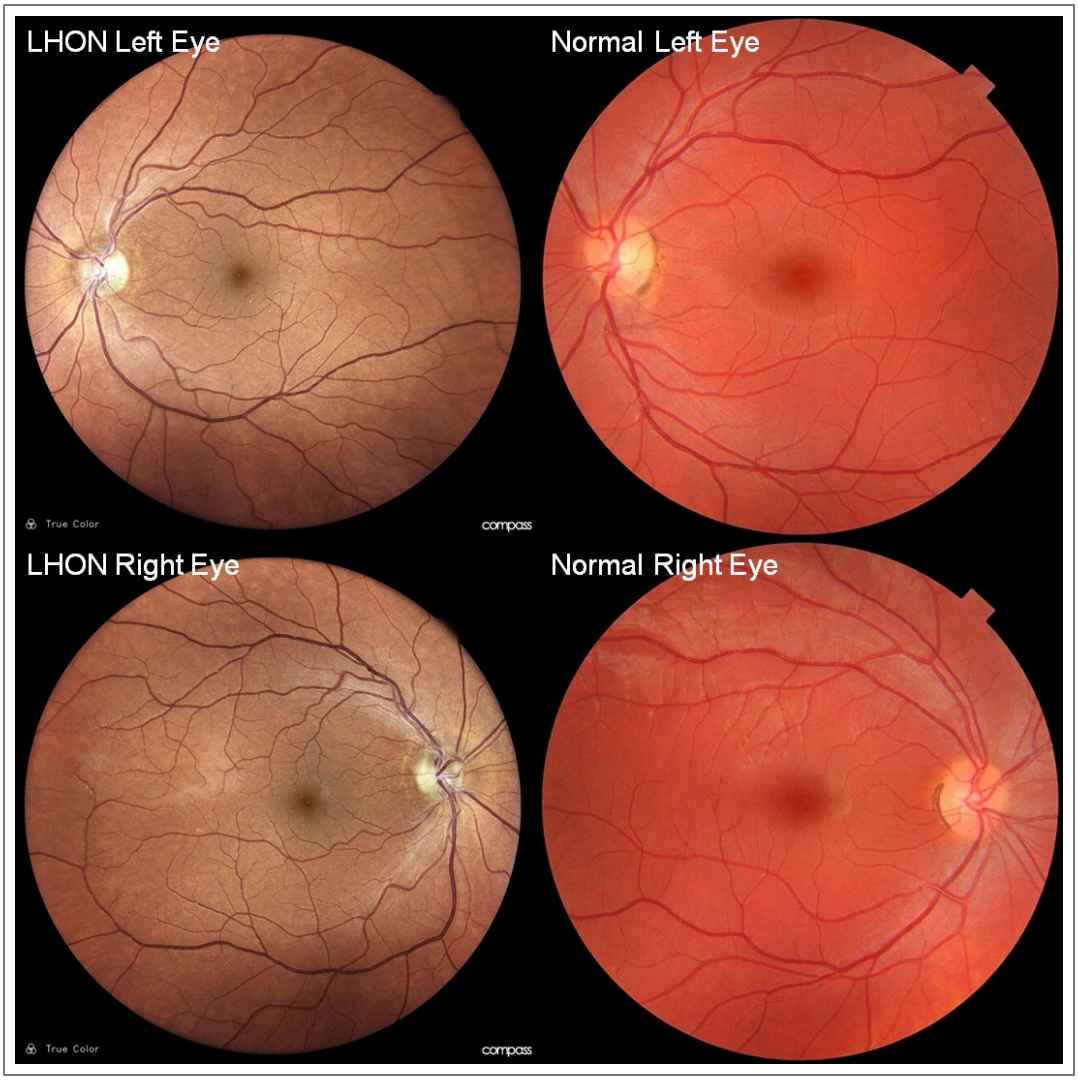

Author response image 1.

We do, however, recognize the importance of linking functional changes to structural alterations (e.g., retinal thickness measured with OCT), and we now highlight this as a key future direction in the discussion. This will be a central focus of a planned follow-up study involving a larger patient cohort.

“Next steps in this work will therefore involve testing larger patient cohorts with diverse forms of vision loss, validating the approach for tracking pathology over time, and investigating how cortex-based visual field measures relate to and complement other visual field and retinal integrity indices including Compass measures and OCT-derived retinal layer thickness.”

“Additionally, linking brain-based variations in function across the visual field to behavioral performance (e.g., perimetry, microperimetry) and retinal structure (fundus imaging, retinal thickness from Optical Coherence Tomography), could help bridge the gap between neural measures and functional outcomes. Such integration would provide deeper insights into developmental, learning, and vision loss mechanisms.”

> *R1-Recommendation 4a: Why is a 0.5 mm smoothing applied to the contrast task data?*

AR-R1-Recommendation 4a: We have now clarified in the Methods section. This 0.5 mm FWHM smoothing kernel was applied to the contrast sensitivity task data to meet the

minimum requirements of the GLM module in SPM.

"To accurately capture neural activity across various eccentricities and polar angle locations, minimal smoothing (0.5mm FWHM Gaussian blur) was applied to the contrast sensitivity task data using FSL's 3dmerge program. This was done to meet the minimum requirements of the GLM module in SPM."

> *R1-Recommendation 4b: Is this the first time the cortical magnification calibration has been applied to the Benson atlas? I recommend including a figure to describe this method.*

AR-R1-Recommendation 4b: This is indeed the first time this correction has been applied to the Benson atlas. We have now added a figure (Figure 3) to illustrate the eccentricity adjustment procedure applied to the Benson atlas.

> *R1-Recommendation 5: In Figure 5, the test-retest reliability can be reported by including r-values.*

AR-R1-Recommendation 5: We have now included Spearman correlation ρ-coefficients for test-retest and between-condition comparisons in Figure 6 (previously Figure 5).

> *R1-Recommendation 6: Inconsistency in the reporting format of statistical values: e.g., the degrees of freedom are presented with, or without parentheses.*

AR-R1-Recommendation 6: Thank you for pointing this out. We have reviewed and standardized the reporting format of all statistical values throughout the manuscript to ensure consistency. Degrees of freedom are now all presented with parentheses, in details:

"Using ANOVA, we found the expected interaction between spatial frequency and eccentricity (F(1.96,11.79) = 28.66, p < 0.001; Figure 4) as well as a main effect of eccentricity (F(2.33,13.99) = 12.67, p < 0.001)."

"We found a main effect of visual field quadrant location on V1 sensitivity (F(2.46,14.76) = 20.71, p < 0.001)."

"Moreover, there was no interaction between spatial frequency and (F(2.16,12.99) = 1.34, p = 0.298), visual field quadrant positions suggesting V1 visual field anisotropies are relatively constant across spatial frequencies."

> ***Reviewer #2 (Public reviews):***
>
> *R2-1a: Questionable sensitivity to differences in patients. The variability in heat maps across healthy control participants is somewhat surprising. Do differences between individuals represent actual visual sensitivity differences, or are they an artifact of the measurement technique, e.g., due to signal-to-noise differences introduced by local variations in brain anatomy? Will the substantial variance across controls allow for a sufficiently stable baseline to detect meaningful differences in individual patients?*

AR-R2-1a: We agree the variability across healthy controls is surprising. It is unclear whether this reflects true individual differences in visual sensitivity or arises from factors like local signal-to-noise introduced by local variations in brain anatomy. It will be really interesting to investigate this further by examining structural variations across the visual field and comparing them with behavioral measures.

As for establishing a stable baseline for patient comparisons, this is inherently an empirical question and depends on the degree of vision loss. LHON patients typically show dense central scotomas (up to 15º) in the chronic phase, making them well suited for detecting sensitivity differences – e.g., between central versus peripheral locations. Detecting subtler

changes – in the acute phase or other conditions – may be more challenging. We agree with the reviewer that a normative range will be essential for contextualizing patient data, which we now mention in the Discussion, and we aim to develop in the future based on the present data.

“Future work will focus on further validating reconstruction accuracy under controlled conditions, including simulated scotomas of varying severity and location, expanding testing to larger patient cohorts, and establishing a normative dataset to contextualize patient data.”

> *R2-1b: Also, as the authors rightly point out, Benson atlas does not model differences along meridians, so upper/lower field differences might not be detectable.*

AR-R2-1b: We acknowledge the limitations of the Benson atlas, particularly its inability to model meridional asymmetries (e.g., upper vs. lower visual field). Still, our goal is to provide a method for tracking visual cortex changes over time. By consistently projecting longitudinal functional data onto the same structural image fitted with the Benson atlas, we maintain a stable anatomical reference, which supports reliable comparisons across timepoints – even with limited spatial accuracy. Future improvements could include shearing corrections, Bayesian updating, or alternative models such as DeepRetinotopy developed by Ribeiro et al.

“Further enhancing the alignment between retinotopic template atlases and individual retinotopic tuning could improve this approach further, for example, by integrating them with functional measures using Bayesian methods (Benson & Winawer, 2018). In parallel, geometric deep learning frameworks such as DeepRetinotopy (Ribeiro et al., 2021) could also offer anatomy-driven predictions from structural MRI, and combining these strategies may yield more accurate and generalizable retinotopic reconstructions.”

> *R2-2: Effects of unstable fixation/eye movements not explicitly tested: The methods state, 'In all tasks, participants were asked to report when the color of a central fixation dot changed', suggesting participants maintained fairly good fixation. Most of the results seem to pertain to measurements where central fixation is required. How does unstable fixation affect measurements?*

AR-R2-2: This is an important point. We have now extensively and systematically investigated the impact of eye movements on the cortical contrast sensitivity maps and updated the Abstract, Methods, Results, and Discussion sections (see R1-1b).

> *R2-3: Potential for clinical translation. Although it is a sensitive measure, functional MRI is costly, is not available in all clinical settings, requires significant post-processing analyses, and may be contraindicated in some individuals due to safety (e.g., metallic implants) or other concerns (e.g., claustrophobia). These could present significant barriers to widespread clinical translation if this were the ultimate goal of the study.*

AR-R2-3: We agree that fMRI, while sensitive, has practical limitations for broad clinical adoption due to cost, accessibility, and contraindications. However, it remains a valuable tool in targeted contexts, where sensitive detection of visual field loss has large utility – for example for evaluating treatment effects in clinical trials. This application has been demonstrated in recent studies (Farahbakhsh et al., 2022; Maimon-Mor et al., 2025; Haal et al., 2016; Ritter et al., 2019).

> *R2-4: Limited range of spatial frequencies. The spatial frequencies tested were still quite low (0.3 and 3cpd) compared to measures such as visual acuity. Extending the measurements to higher spatial frequencies could allow better characterization of central vision, although necessarily for peripheral vision.*

AR-R2-4: We agree that extending to higher spatial frequencies could improve central vision characterization and note this can be readily incorporated into future studies using the

current framework. However, LHON patient's acuity tends to be very low, and we found that 5cpd did not allow us to measure any cortical contrast sensitivity in a prior pilot. So, to characterize the visual field in LHON with fMRI, we therefore aimed to balance central and peripheral coverage: 0.3 cpd ensured broad detectability, while 3 cpd offered a middle ground to assess central vision without exceeding acuity of this population. Additional approaches, such as neural contrast sensitivity functions (e.g., Roelofzen et al., 2025) may also offer complementary insights such as acuity, and contrast sensitivity across the full spatial frequency range (area under the curve).

> ***Reviewer #2 (Recommendations for the authors):***
>
> *R2-Recommendation 1: It appears that the reliability measures, comparing differences in Spearman correlations between and within sessions, were not tested statistically, but evaluated qualitatively. What was the justification for this? The results only state Spearman values, but the discussion claims that the differences between the two comparisons were significant.*

AR-R2-Reconmandation 1: The differences in Spearman correlations between and within sessions were tested statistically, and the omission of p-values was an oversight. We have now revised the Results section results from the paired one-tail t-test as follows:

"We collected test-retest reliability measures from 4 out of 7 participants (Figures 6A-B) and benchmarked them against the correlations between the 0.3cpd condition and 3cpd spatial frequency condition, collected in the same session (Figure 6C). If measures are reliable, correlations should be higher for repeated measures with the same spatial frequency stimulus, collected on different days. We tested this prediction using a one-tailed paired t-test."

"This difference was statistically significant ($t(3) = 2.62$, $p < 0.0395$)."

> *R2-Recommendation 2a: The variability of heat maps (visual field sensitivities) between healthy controls should also be discussed. What are potential explanations for this variability?*

AR-R2-Recommendation 2: We have expanded the Discussion section to address the variability observed in cortical sensitivity maps across healthy controls.

"We also observed intriguing variability in cortical visual field maps across healthy controls, and this variability was consistent across measures. This may reflect genuine individual differences in visual sensitivity that are relevant for behavioral performance. Alternatively, it could arise from factors such as local signal-to-noise differences driven by anatomical variability. However, the fact that maps derived from different spatial stimulus conditions showed markedly different patterns argues against a purely anatomical explanation and suggests that at least part of the variability is functional. Despite this inter-subject variability, variations in cortical contrast sensitivity across eccentricities and visual field quadrants were significant at the individual level indicating high sensitivity."

> *R2-Recommendation 2b: There should also be more discussion about any potential effects of eye movements/unstable fixation in order to address the suitability of the methods for these clinical populations.*

AR-R2-Recommendation 2b: Please refer to our response to R2-2, where we also detail the corresponding changes made in the manuscript.

> ***Reviewer #3 (Public review):***
>
> *R3-1: The authors should more strongly emphasize their findings on the organization of contrast sensitivity, particularly in light of the stimulation extent provided by the wide-*

> *field setup.*

AR-R3-1: Thank you for this important point – we have now emphasized more clearly in the manuscript that our method extends the measurement of contrast sensitivity to 20º eccentricity, which represents a significant advancement over previous studies.

"These results demonstrate that our approach can detect subtle changes in visual sensitivity across eccentricities at the individual participant level. The ability to reveal these gradients was made possible by the large peripheral coverage provided by our large-field stimulation set-up (see Figure A1 in Appendix section), which enabled a more complete characterization of V1 sensitivity across the visual field. Importantly, the same effects were preserved when using retinotopic estimates derived from structure-based atlases, demonstrating that atlas-based methods can be used as alternative to pRF mapping in cases where it might otherwise be difficult or impossible to directly collect pRF measures. Together, these highlight both the validity of our approach and its potential to broaden the scope of visual neuroscience."

"Crucially, the ability to visualize these sensitivity gradients was made possible by the large peripheral coverage provided by our large-field stimulation set-up. Such coverage is particularly important for clinical applications, as it enables the detection of visual field losses beyond the macula (i.e., beyond 10º eccentricity) and the evaluation of residual peripheral vision in patients with macular-restricted damage. In doing so, this work provides a useful tool for advancing both basic visual neuroscience and translational research in clinical populations."

> *R3-2: Certain methodological aspects require further clarification, particularly regarding the correction of eccentricity values from the Benson atlas. It's not clear which V1 masks are used for the specific analysis which could have a substantial impact on the reported differences between the two approaches of pRF mapping and atlas-based pRF parameters.*

AR-R3-2: The correction of eccentricity values was performed using the V1 label provided by the Benson atlas. We have now explicitly stated this in the Methods section:

"We collected data from 7 healthy controls (mean±SD: 29.6±4.7yo; 1M). All controls either had normal or corrected to normal vision, with no other ocular pathologies, and were recruited from the local staff and student pool at the University College of London. Each control completed both the population receptive field (pRF) mapping and the fMRI contrast sensitivity task. To assess measurement repeatability, four participants (C2, C4, C5, C6) performed the contrast sensitivity task twice. Additionally, one participant (C5) repeated the task under two simulated vision loss conditions (ring or quadrant loss), and two others (C5, C6) completed it with different levels of eye movement."

"Four participants (C2, C4, C5, C6) were invited for a second session in which they repeated the task to assess the reliability of the measures."

> *R3-4: The conclusion that high-contrast patterns as in pRF mapping are not optimal to test for subtle but potentially clinically relevant changes in the visual field coverage is very valid. The suggested use of contrast sensitivity can therefore be a potentially well-suited parameter for estimating visual field losses. The presented work is an interesting starting point and the proposed method of using contrast sensitivity as a measure for partial vision loss should further be explored.*

AR-R3-4: Thank you for the positive evaluation of our work.

> ***Reviewer #3 (Recommendations for the authors):***

> *R3-Recommendation 1: The shown organization of contrast sensitivities is consistent with previous studies; however, it extends the measurements to up to 20° eccentricity, which is, to my knowledge, much more than previously reported. The authors should therefore emphasize this more strongly.*

AR-R3-Recommendation 1: Please refer to our response to R3-1, where we also detail the corresponding changes made in the manuscript.

> *R3-Recommendation 2: In the Methods section, it is not entirely clear why the eccentricity values originating from the Benson atlas need to be corrected using Horton & Hoyt cortical magnification. Do the authors consider these cortical magnification measurements as ground truth? Is the correction only applied to higher eccentricity values that are not mapped by the Benson atlas?*

AR-R3-Recommendation 2: The Benson et al. (2014) atlas predicts both polar angle and eccentricity from cortical anatomy (curvature, thickness) using a template pRF dataset and a mathematical retinotopic model. However, it does not incorporate a smooth parametric cortical magnification function such as Horton & Hoyt. Because the atlas is fit to an average map across subjects, and because the FreeSurfer alignment used to apply the template cannot incorporate functional information, the atlas cannot capture individual variability in eccentricity or cortical magnification. In practice, we therefore treat the Benson atlas as providing the correct topological layout of eccentricity, but not necessarily the correct eccentricity values for a given individual. Moreover, the data used to generate the Benson atlas have mainly been restricted to the central visual field (roughly 8°-12°) and the Benson atlas themselves has never been fit with data more eccentric than 20°. Consequently, peripheral eccentricity values are more model-driven and less constrained by ground-truth data.

To improve the correspondence between the atlas and expected cortical representations, we applied Horton & Hoyt cortical magnification function to all eccentricities in the V1 Benson mask (from the foveal confluence to the periphery, up to 90°). We assume that the Horton & Hoyt model, adapted from physiology data, provides an accurate model of group level cortical magnification (Benson et al., 2021) – even though it does not capture individual differences. This means it offers the best approximation of ground-truth in the absence of individual pRF data, which is often not feasible to collect in patients with unstable fixation. We have now added a figure that showcases the method and shows how this correction affects the distribution of eccentricity values in the Benson atlas.

> *R3-Recommendation 3: For the analysis using the atlas-based retinotopy, it is not entirely clear whether the authors also use the provided V1 masks. In other words, differences between the original pRF-based and atlas-based analyses could originate from different borders of V1 rather than from the atlas-based pRF parameters. The authors could try using the same mask for both analyses, either the manually delineated one or the atlas-based one.*

AR-R3-Recommendation 3: This is a well-noted point that is important to clarify. We used a manually delineated V1 mask for the own pRF map data and the Benson mask for the adjusted Benson atlas-based analysis – both restricted to the screen size. The difference in included vertices could have indeed introduced some additional error beyond the atlas/pRF mapping itself. We have opted not to correct this in this version of the manuscript because (1) the error introduced is likely small (as we inspected that the alignment of V1 ROI delineations with the Benson ROIs are good, so effects are likely not too major - although using identical masks may slightly improve the mapping further in particular the very center and outer-periphery), and (2) our ROI selection for each respective approach is in line with typical procedures used in reality. Critically, the spatial gradients in cortical contrast sensitivity are

preserved across the pRF and Benson atlas approach with the different ROIs, so we believe that improvements would not alter our conclusions that Benson offers a useful alternative when pRF mapping is not possible - however, we now highlight this important difference across the two approaches in the paper.

“With this structure-based atlas, we successfully replicated key variations in visual field function (across eccentricity and polar quadrants), although sensitivity to more subtle differences (e.g., upper versus lower quadrant anisotropy) was reduced. This reduction may partly stem from differences in ROI definitions: a manually delineated V1 mask was used for the pRF-based data, while the Benson atlas mask was used for the adjusted Benson atlas analysis. Such differences could introduce minor error beyond the atlas/pRF mapping itself due to differences in the vertices included by each mask.”

“Importantly, the spatial gradients in cortical contrast sensitivity were preserved across both the pRF and Benson atlas approaches, indicating that minor ROI differences do not affect our conclusions. Together, these findings show that the Benson atlas remains a useful alternative when pRF mapping is not feasible.”

> *R3-Recommendation 4: The patient was measured monocularly. Given the widefield stimulation setup and the fact that the blind spot is located at about 15° eccentricity, do the authors expect to measure this blind spot with the given setup?*
>
> *Does this have an influence in binocular measurements?*

AR-R3-Recommendation 4: This is an interesting point. In theory, our wide-field setup could allow for the detection of the blind spot, as located around 12-15° eccentricity. However, in our LHON patient, the visual field defect typically extends to or beyond the blind spot, making it difficult to isolate its boundary, as shown in Figure 11 (previously Figure 7). Additionally, under binocular viewing, the brain integrates inputs from both eyes to create a unified percept, which may obscure blind spots unless specific paradigms are used (e.g., binocular rivalry or dichoptic tasks). Whilst this is outside the scope of this work, our setup could be adapted to map out the blind spot or explore phenomena like binocular rivalry more directly in future research.

> *R3-Recommendation 5: How stable is the presented wide-field stimulation setup? In other words, does the eye tracker still capture the eye reliably after small head movements?*

AR-R3-Recommendation 5: While small head movements can occur, these were minimized by the use of padding cushions and monitored throughout the session, and the eye tracker maintained reliable tracking throughout the sessions.

> *R3-Recommendation 6: Are the shown sine-wave gratings always oriented the same? We would expect orientation tuning curves in the early visual cortex; how could this influence the results?*

AR-R3-Recommendation 6: For six of the seven control participants (C1-C6), the sinewave gratings were presented with a fixed horizontal orientation. In an updated version of the task – used for participant C7, cases of simulated eye movements, cases of artificial scotoma, and the patient – the orientation of the gratings was varied every 5 seconds among four angles (−45°, 0°, 45°, 90°) during each 15-second stimulus block.

We acknowledge that orientation tuning in the early visual cortex could influence responses, since V1 neurons are selective for specific stimulus orientations and respond most strongly to their preferred orientation. However, we replicated the same overall pattern of results in groups tested with a single orientation and with multiple orientations. Importantly, some participants completed both versions of the task, and the contrast sensitivity patterns remained consistent across conditions. This suggests that the results we report are robust

across different orientation-tuned populations for the purposes of this study. A more fine-grained investigation of orientation effects would nevertheless be an interesting direction for future work.

“For six control participants (C1–C6), gratings were initially presented with a fixed horizontal orientation. In an updated version of the task – used for C7, cases of simulated eye movement, cases of artificial scotoma, and the LHON patient – the orientation varied every 5 s among four angles (−45º, 0º, 45º, 90º). Contrast sensitivity patterns were consistent across single and multiple-orientation conditions, including in participants who completed both versions, indicating robustness across orientation-tuned populations.”

> *R3-Recommendation 7: Are pRF centers also fitted outside the stimulated 20º radius? If yes, were they masked for the analysis?*

AR-R3-Recommendation 7: During pRF model fitting, pRF centers were allowed to extend beyond the stimulated visual field, up to approximately 1.5 times the maximum stimulus eccentricity (~30°), to improve model stability near stimulus boundaries. Eccentricity was sampled on a logarithmically spaced grid defined as 2^{*}, with x ranging from -5 to 0.6 in steps of 0.2, and then scaled by the maximum stimulus eccentricity (20°) to express pRF centers in degrees of visual angle. This spacing approach provided finer sampling near the fovea and progressively coarser sampling at larger eccentricities, consistent with cortical magnification principles. For all subsequent analyses of cortical contrast sensitivity, pRF centers located outside the stimulated 20° eccentricity were explicitly excluded. Likewise, although the Benson atlas provides eccentricity estimates extending well beyond the stimulated range (up to ~90°), only pRF centers within 20° were included to ensure consistency across pRFbased and atlas-based analyses.

“During pRF model fitting, pRF centers were allowed to extend beyond the stimulated visual field to improve model stability near stimulus boundaries – up to approximately 1.5 times the maximum stimulus eccentricity (~30°). Eccentricity was sampled on a logarithmically spaced grid defined as 2*, with x ranging from −5 to 0.6 in steps of 0.2, and then scaled by the maximum stimulus eccentricity (20°) to express pRF centers in degrees of visual angle. This sampling scheme provided finer resolution near the fovea and progressively coarser sampling at larger eccentricities, consistent with cortical magnification principles.”

“For all subsequent analyses of cortical contrast sensitivity, pRF centers outside the stimulated 20° eccentricity were excluded. Similarly, although the Benson atlas provides eccentricity estimates extending far beyond the stimulated range (up to ~90°), only values within 20° were retained to maintain consistency across pRF-based and atlas-based analyses.”

> *R3-Recommendation 8: L212: Could the authors please clarify what "scaled across eccentricity to account for cortical magnification" means for the given stimulus?*

AR-R3-Recommendation 8: The pRF stimulus was scaled across eccentricity using a logarithmic transformation of retinal radius to approximate cortical magnification. Radial checker boundaries were defined in log eccentricity space *(log(r))*, resulting in an exponential increase in checker size with eccentricity (scaling factor = 3.2; ~1.37× increase per radial step). As a result, the spatial frequency content of the stimulus decreases with eccentricity (i.e., checker size increases), compensating for known changes in V1 spatial frequency preference across the visual field. This eccentricity dependent scaling inherently relies on precise fixation to stimulate the intended retinal locations, which can be difficult for patients with central vision loss and therefore motivates the use of Benson templates.

“This scaling was implemented by applying a logarithmic transformation of retinal radius, such that radial checker boundaries were defined in log eccentricity space *(log(r))*, where r denotes to eccentricity relative to the fixation target). This produced an exponential increase

in checker size with eccentricity (scaling factor = 3.2; ~1.37 times increase per radial step), resulting in lower spatial frequency content at larger eccentricities – consistent with known variations in V1 spatial frequency tuning. Because this eccentricity dependent scaling assumes precise fixation, it can be challenging for individuals with central vision loss, further motivating the use of Benson atlas templates in such populations."

> *R3-Recommendation 9: L213: Three runs were measured per session, were they averaged before analysis or analyzed independently? If analyzed independently, how were the individual results handled?*

AR-R3-Recommendation 9: As described in the Methods, data from all three runs were first aligned to an alignment scan that had been co-registered to the MPRAGE image – typically the scan with the fewest outlier voxels, or alternatively, a single-band reference scan in cases of misregistration. The runs were then analyzed as separate regressors in a single design matrix in SPM to account for run-specific variation - following standard recommendations for this software (Author response image 2 shows the SPM design matrix for the GLM). We did not average the runs beforehand due to differences in the order of stimulus presentation across runs. Instead, the GLM modeled each run's specific presentation sequence to estimate condition-specific beta values, capturing the average contribution of each spatial frequency and contrast level to the BOLD response.

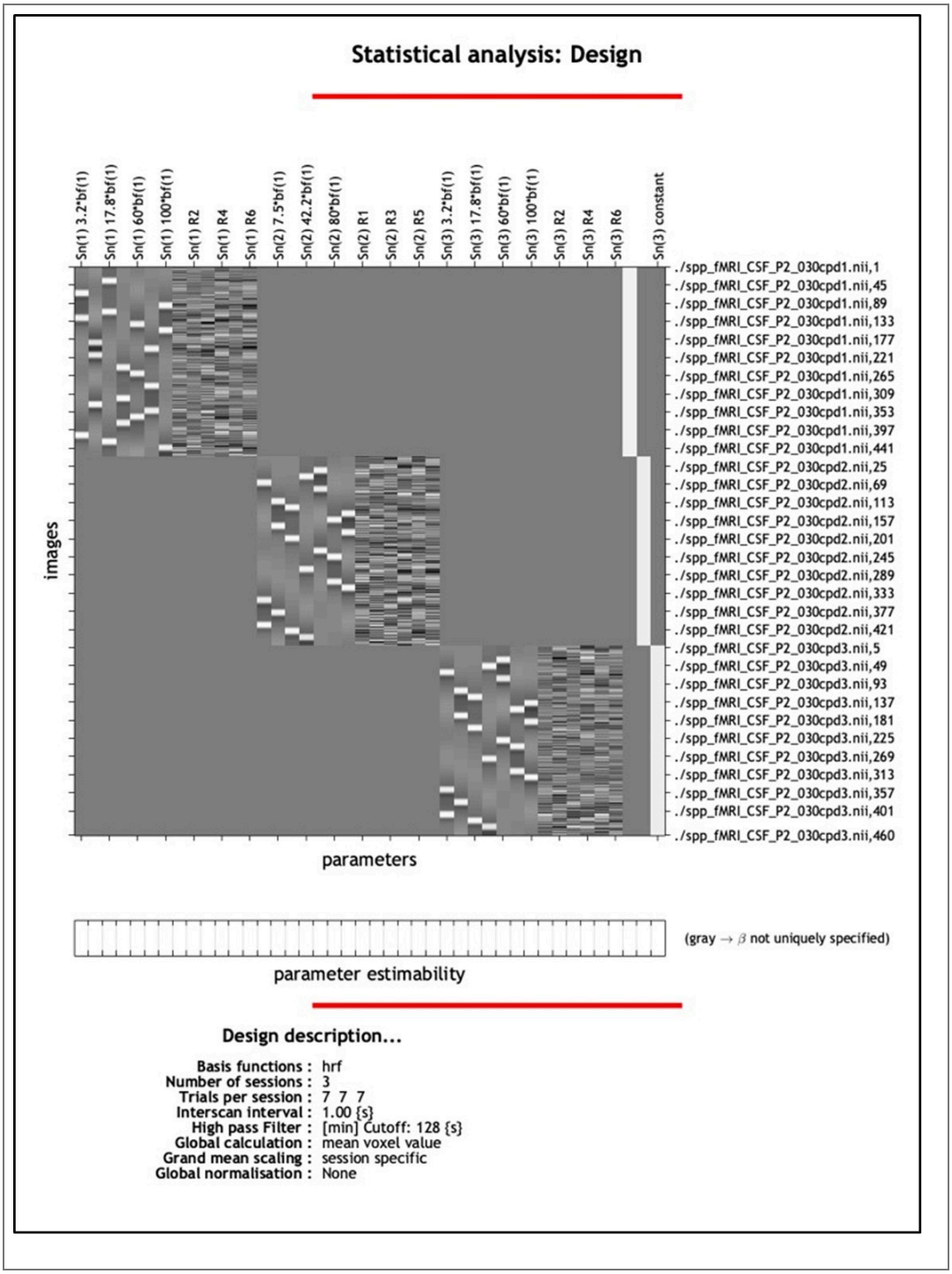

Author response image 2.

> *R3-Recommendation 10: L289: Did the authors check for very small pRF sizes, as SamSrf is prone to fitting many small sizes?*

AR-R3-Recommendation 10: We did not apply an explicit filter to remove very small pRF sizes; we excluded only pRFs with $\sigma > 6$.

> *R3-Recommendation 11: L384: p is missing before the value.*

AR-R3-Recommendation 11: Thank you for catching this oversight. We have now added the missing p-value in the revised manuscript.

"Post-hoc tests using Holm-Bonferroni correction show that V1 neuronal populations receiving inputs from the central visual field (0.5-4.5°) showed greater contrast sensitivity to high spatial frequency as compared to low spatial frequency stimuli (steeper slope for the 3cpd versus 0.3cpd condition: 0.5-2.5°: $t(6) = 4.35$, $p_{bonf} = 0.0149$; 2.5-4.5°: $t(6) = 3.471$, $p_{bonf} = 0.0266$)."

> *R3-Recommendation 12: I have a very subjective comment regarding the figures. I do not really like the use of the hot colormap in this setting, as I feel it is hard to interpret high and low values.*

AR-R3-Recommendation 12: We appreciate the suggestion, but we have had many heated discussions amongst the authors about this and have moved back forth several times before settling. Hopefully the reviewer will be happy for us to stick with the author's eventually agreed-on subjective preference although we acknowledge that it is by no means a perfect color scheme.

> *R3-Recommendation 13: L474: Suddenly, a second session appears in the Results section; please report this in Methods.*

AR-R3-Recommendation 13: Please refer to our response to R3-3, where we also detail the corresponding changes made in the manuscript.

> *R3-Recommendation 14: Figure 5C: are the reported results from the first session of the same subjects?*

AR-R3-Recommendation 14: That is correct. The results shown in Figure 6C (previously 5C) reflect correlations between slope estimates obtained from the 0.3 and 3cpd conditions within the same session for each subject. We have updated the panel title to "C. 0.3cpd vs 3cpd (within session)" to clarify this point.

> *R3-Recommendation 15: For the classic pRF mapping (Figure 6D), the artificial scotoma shows lower contrast sensitivity within the scotoma and increased values outside its borders. In contrast, using the retinotopic template (Figure 6E), the area of increased sensitivity is shifted inside the scotoma. Can the authors please comment on this discrepancy?*
>
> *Is this shift due to systematic differences between the eccentricity values estimated during the pRF run and those derived from the template?*
>
> *If such a shift exists, is it induced by the eccentricity correction step performed?*

AR-R3-Recommendation 15: The shift inside the scotoma observed in the atlas-based analysis (Figure 9E; previously Figure 6E) compared to the pRF-based analysis (Figure 9D; previously Figure 6D) likely reflects residual inaccuracies in eccentricity estimates from the adjusted Benson atlas. While the Horton & Hoyt correction improves the alignment of eccentricity values, it does not ensure perfect matching with the pRF data. Without the Horton & Hoyt correction, the misalignment and shift of activity in the scotoma region are even more pronounced (see below).

We have added a sentence to the Methods section to justify the applied correction. Furthermore, to illustrate the impact of misalignment and its correction on cortical sensitivity maps, we have included an additional figure in the Appendix section showcasing the effect of applying the correction to improve mapping of the artificial scotoma.

"We initially observed inaccuracies between the template and individual retinotopy eccentricity estimates which led to substantial distortions in cortical visual field maps due to

cortical magnification – especially in peripheral locations (see Figure A4 in Appendix section)."

> *R3-Recommendation 16: L532: The age and mutation type of the patient are already reported in the Methods. In general, many Methods and Discussion statements are embedded within the Results section.*

AR-R3-Recommendation 16: We are aware that it is a stylistic choice to remind of method in the results and foreshadow discussion. We chose this approach to support the interpretability of the results for less specialist readers.

> *R3-Recommendation 17: L636: Did the authors consider other options for estimating pRF parameters based on anatomical features, like Ribeiro et al. (2021;https://github.com/felenitaribeiro/deepRetinotopy_TheToolbox).*

AR-R3-Recommendation 17: We agree that alternative approaches to estimating pRF parameters based on anatomical features, such as the DeepRetinotopy method proposed by Ribeiro et al. (2021), are promising and worth exploring. In this study, we used the Benson atlas as a starting point, along with an adjustment of eccentricity estimates based on cortical magnification. Future work could compare the performance of different retinotopic template fitting approaches, including deep learning-based methods, to further improve anatomical alignment and functional predictions.

"Further enhancing the alignment between retinotopic template atlases and individual retinotopic tuning could improve this approach further, for example, by integrating them with functional measures using Bayesian methods (Benson & Winawer, 2018). In parallel, geometric deep learning frameworks such as DeepRetinotopy (Ribeiro et al., 2021) could also offer anatomy-driven predictions from structural MRI, and combining these strategies may yield more accurate and generalizable retinotopic reconstructions."

> *R3-Recommendation 18: Figure A4: This figure brings up a very important point, namely, whether small eye movements reduce the accuracy of pRF and contrast sensitivity estimates. However, these experiments and results are not reported in the manuscript. I would prefer the authors to add all necessary Methods and Results, or at least not leave this Figure unexplained.*

AR-R3-Recommendation 18: We thank the reviewer for highlighting the importance of this figure. To address this point, we collected additional data and have revised the manuscript to include a dedicated section on the effects of eye movements, with corresponding updates in the Abstract, Methods, Results, and Discussion.

https://doi.org/10.7554/eLife.105930.2.sa0